

Electronic Supporting Information

Synthetic Diversity and Change in Nuclearity in [Co-Dy] Coordination Aggregates: Bridge Removal, Solvent Induced Structural Reorganization and AC Susceptibility Measurements

Dipmalya Basak,^a Jan van Leusen,^b Tulika Gupta,^c Paul Kögerler,^b Debashis Ray^{*a}

^aDepartment of Chemistry, Indian Institute of Technology, Kharagpur 721 302, India

^bInstitute of Inorganic Chemistry, RWTH Aachen University, D- 52074 Aachen, Germany

^c Department of Chemistry, Institute of Science, Banaras Hindu University, Varanasi 221005, India

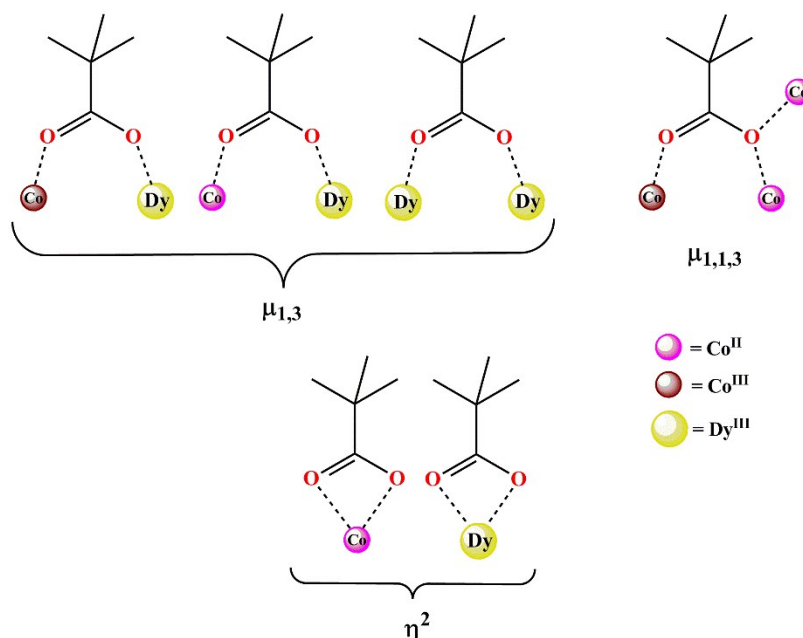
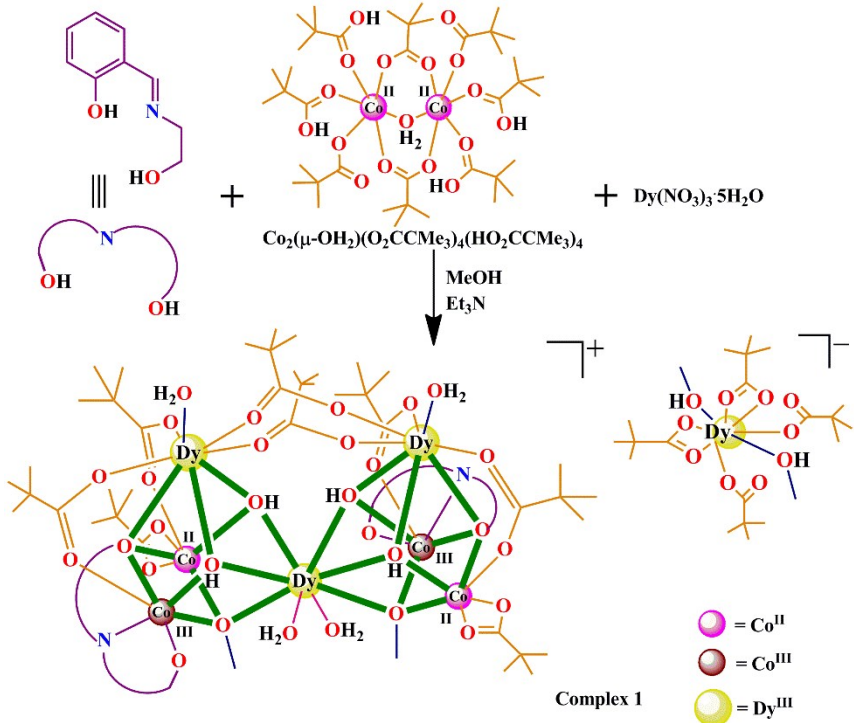


Chart S1. Different binding modes of pivalate ions found in this work.



Scheme S1. Synthesis of **1**.

Description of dicubane core of **1**

Within the $\{\text{Co}_2\text{Dy}_2\}$ cube the shortest intermetallic separation is observed between $\text{Co1}\cdots\text{Co2}$ at $3.1099(3)$ Å, where the former is bivalent and later is present as trivalent ion (Figure 3). The longest separation amounts to $3.8802(2)$ Å for $\text{Dy1}\cdots\text{Dy2}$ (both eight-coordinate). The distorted O_8 coordination environment around each Dy^{III} ion leads to a strong distortion in the cube structure. One of the triangular faces of square-antiprism structure around Dy2 comprising of O_3 , O_4 and O_{15} is utilized for the formation of this cube. On the other hand, Dy1 at the vertex-shared position, share two triangular faces consisting of O_4 , O_5 and O_{15} to two cubes. The remaining two coordination sites around Dy1 are occupied by two water molecules. Of the four DyCoO_2 faces, the separation between the doubly-bridged Dy1 and Co centers are longer ($\text{Dy1}\cdots\text{Co1}$, $3.4484(15)$ Å; $\text{Dy1}\cdots\text{Co2}$, $3.4604(13)$ Å) as compared to the separation between triply bridged Dy2 and Co centers ($\text{Dy2}\cdots\text{Co1}$, $3.4130(15)$ Å; $\text{Dy2}\cdots\text{Co2}$, $3.3850(15)$ Å) due to the presence of carboxylate ions as third bridge in the later cases. The separation between the Dy^{III} ions on the two corners of two separate cubes ($\text{Dy2}\cdots\text{Dy2}$) is $4.8284(4)$ Å, much longer than the $\text{Dy1}\cdots\text{Dy2}$ separations within the cubes.

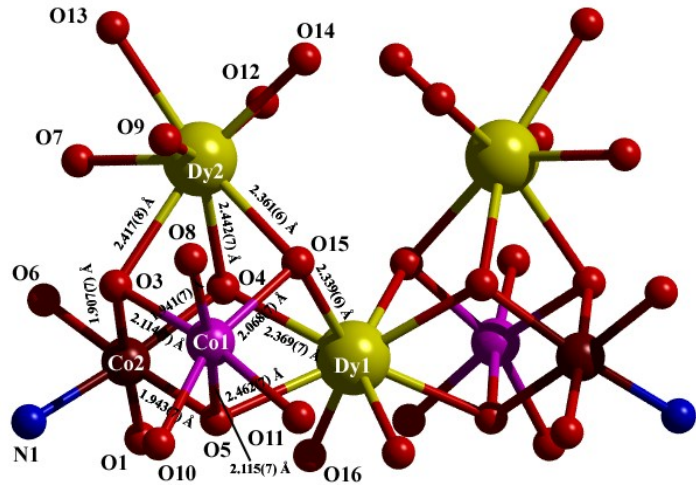


Figure S1. Core structure of **1** depicting the different bond distances. Carbon and hydrogen atoms omitted for clarity. Color code: Red, oxygen; blue, nitrogen; yellow, dysprosium; pink, cobalt(II); brown, cobalt(III).

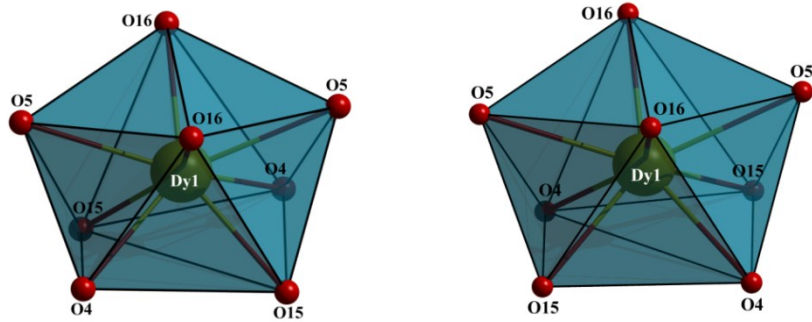


Figure S2. Coordination geometry around Dy1; distorted triangular-dodecahedron in **1** (left) and distorted square-antiprism in **2** (right).

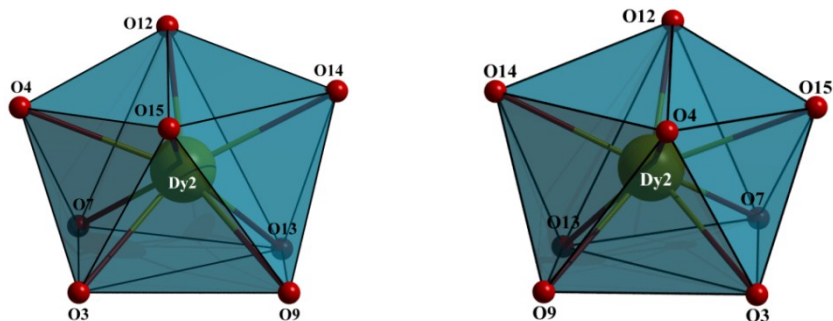


Figure S3. Distorted square-antiprism coordination geometry around Dy2 in **1** (left) and **2** (right).

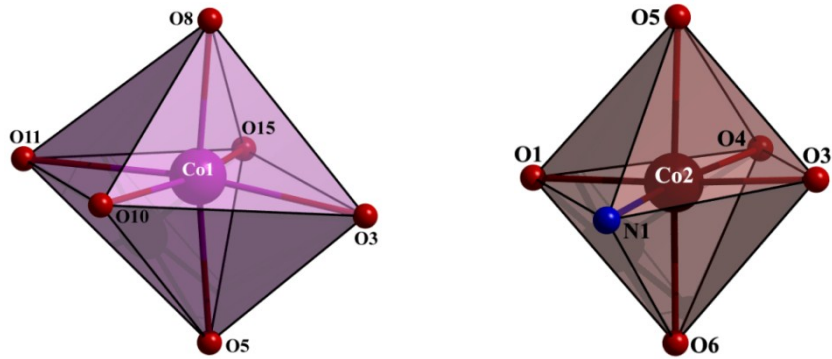


Figure S4. Distorted octahedral coordination geometry around Co1 (left) and Co2 (right) in **1**.

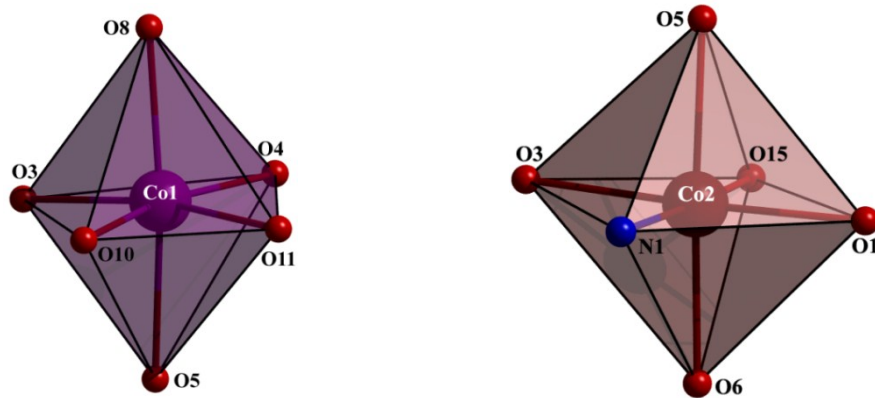


Figure S5. Distorted octahedral coordination geometry around Co1 (left) and Co2 (right) in **2**.

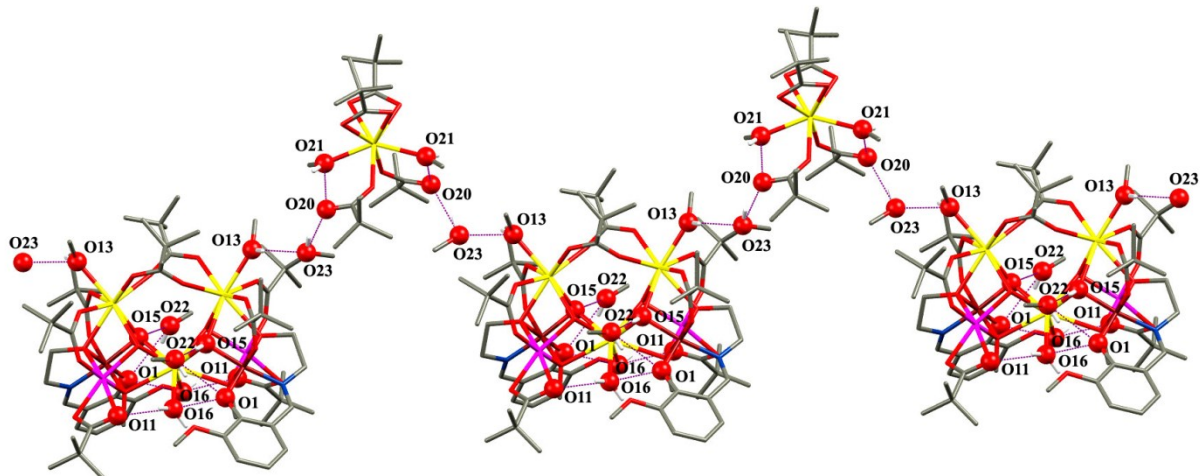


Figure S6. Trapping of unique $\text{Dy}^{\text{III}}(\eta^1\text{-O}_2\text{CCMe}_3)_2(\eta^2\text{-O}_2\text{CCMe}_3)_2(\text{MeOH})_2^-$ anion and solvent molecules through hydrogen bonding interactions forming a 1D chain structure in **2**.

Description of hexanuclear core of **3**

Inside the hexanuclear $\{\text{Dy}^{\text{III}}_2\text{Co}^{\text{II}}_2\text{Co}^{\text{III}}_2\}$ structure the longest intermetallic separation equals 3.8635(2) Å between $\text{Co}2\cdots\text{Dy}1$ connected by $\mu_3\text{-OH}^-$ bridges, whereas the shortest distance is observed between $\text{Co}2\cdots\text{Co}2$ at 3.2213(1) Å, bridged by the two O atoms from two $\mu_{1,1,3}^-$

O_2CCMe_3 groups (Figure 9). The separation between $\text{Co1}\cdots\text{Co2}$, bridged by $\mu_3\text{-OH}^-$, is found to be the second longest at $3.5895(2)$ Å, whereas the $\text{Co1}\cdots\text{Co2}$ separation having a $\mu_2\text{-O}_{\text{alk}}$ (alk = alkoxido) bridge is shorter at $3.4887(2)$ Å. The doubly-bridged diamond core involving $\mu_3\text{-OH}^-$ and $\mu_2\text{-O}_{\text{Ph}}$ (Ph = phenoxido) bridges has the second shortest intermetallic separation of $3.3986(5)$ Å between $\text{Co1}\cdots\text{Dy1}$. The overall disposition of the six metal ion centers of two types is more or less planar as opposed to the cubic arrangements found in **1** and **2** with both the two Co2 centers slightly displaced by 0.390 Å above and below the plane containing Co1 and Dy1 centers (Figure S8). The bridging O atoms of $\mu_3\text{-OH}^-$ groups are displaced by 0.328 Å from the plane while those of $\mu_2\text{-O}_{\text{Ph}}$ lie 0.715 Å away from the plane. The μ_2 -bridging O atoms of $\mu_{1,1,3}\text{-O}_2\text{CCMe}_3$ sits 1.377 Å above and below the plane, with $\mu_2\text{-O}_{\text{alk}}$ at a distance of 0.756 Å.

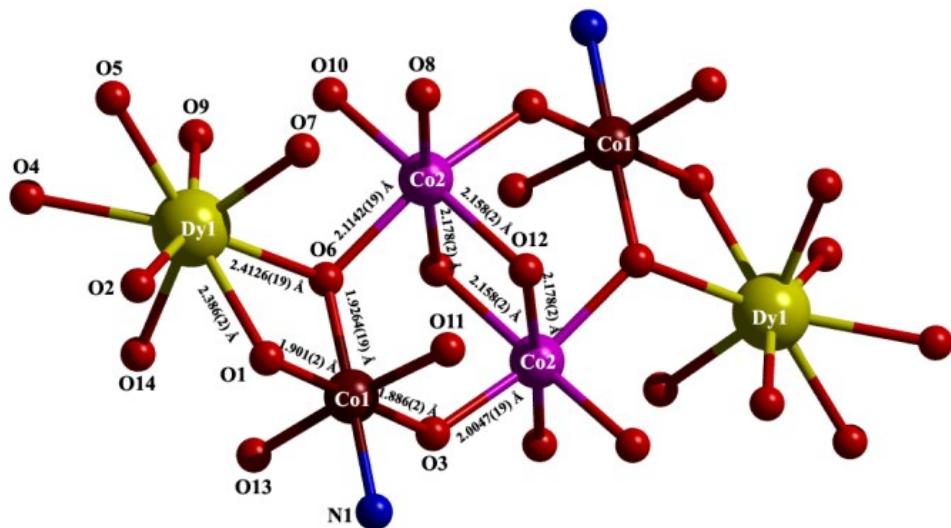


Figure S7. Core structure of **3** depicting the different bond distances. Carbon and hydrogen atoms omitted for clarity. Color code: Red, oxygen; blue, nitrogen; yellow, dysprosium; pink, cobalt(II); brown, cobalt(III).

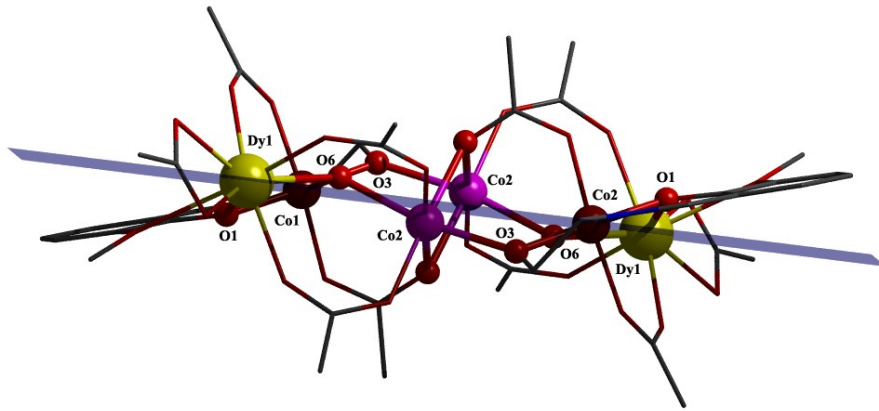


Figure S8. Positioning of metal ion centers and bridging O atoms with respect to the plane (lilac blue) containing two Dy1 and two Co1. Methyl groups of pivalate anion and hydrogen atoms are omitted for clarity. Color code: Red, oxygen; blue, nitrogen; yellow, dysprosium; pink, cobalt(II); brown, cobalt(III).

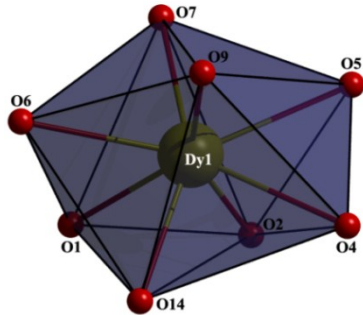


Figure S9. Distorted trigonal dodecahedral coordination geometry around Dy1 in **3**.

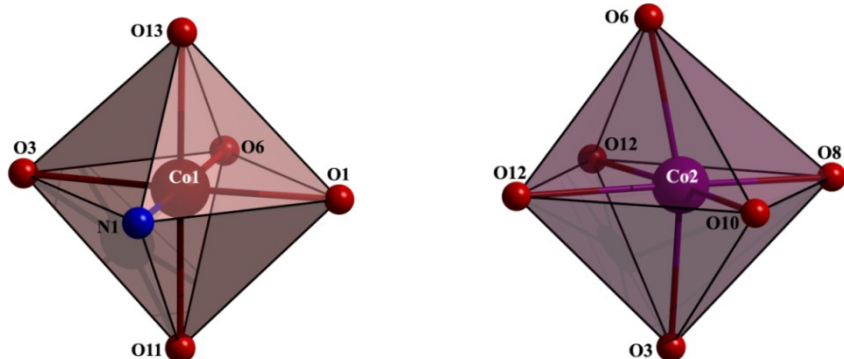
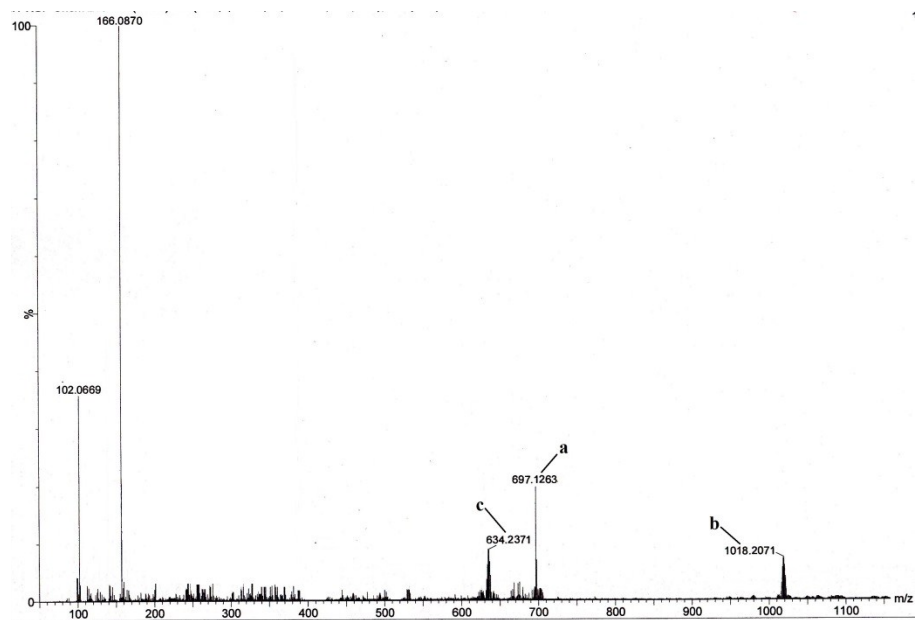
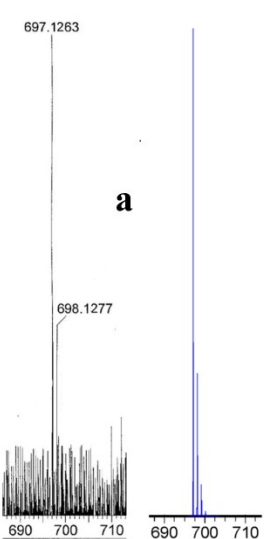


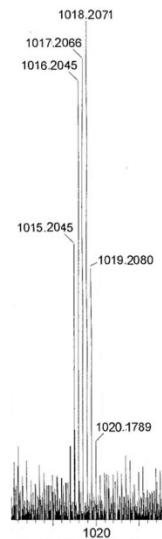
Figure S10. Different level of distortion of octahedral coordination geometry around Co1 (left) and Co2 (right) in **3**.



Experimental Simulated



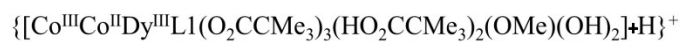
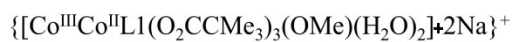
Experimental



Simulated

a

b



Experimental Simulated

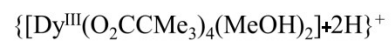
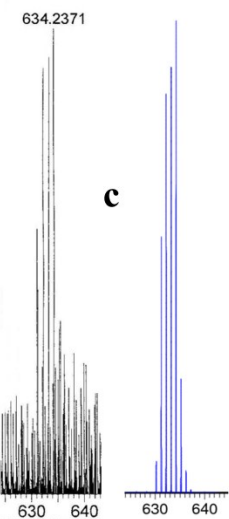
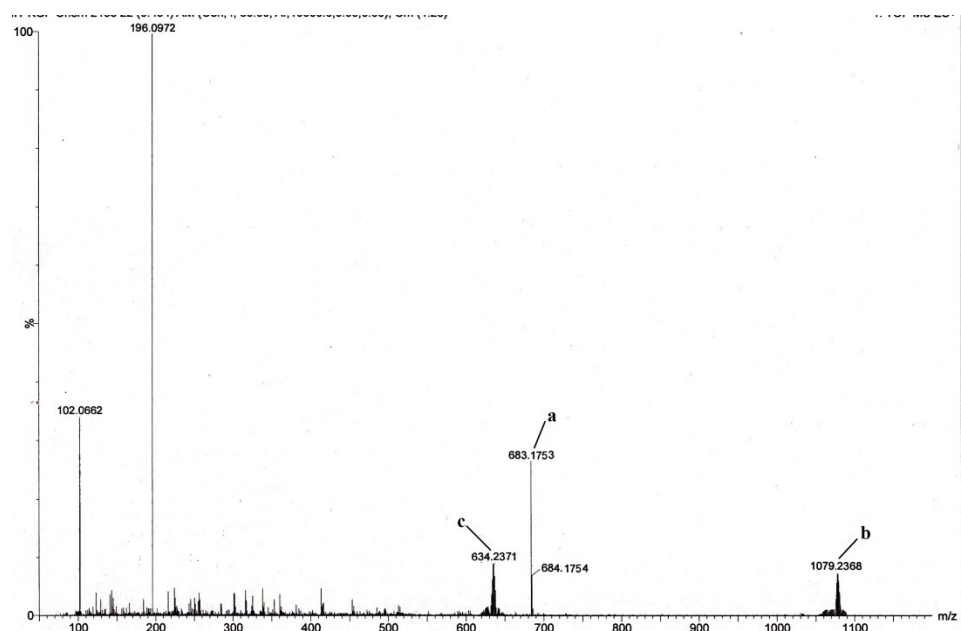
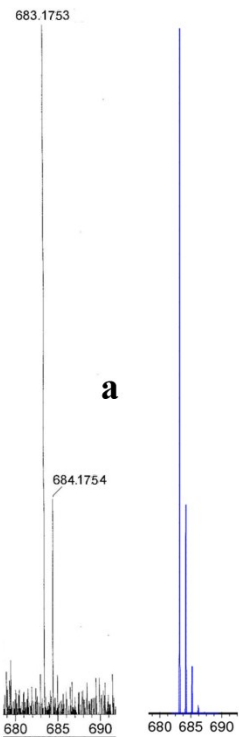


Figure S11. Experimental and simulated peaks obtained from HRMS (+ve) of **1** in MeOH corresponding to different species present in solution.

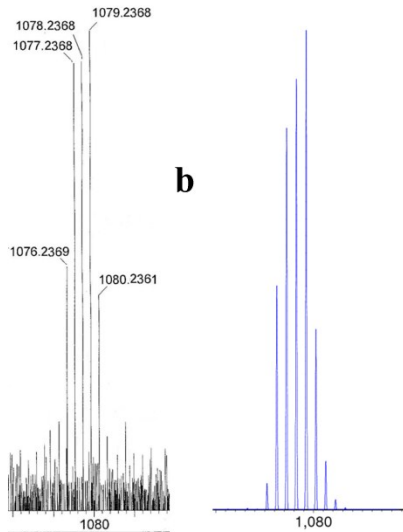


Experimental Simulated

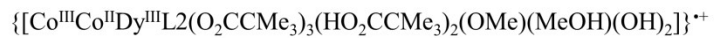
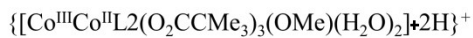


a

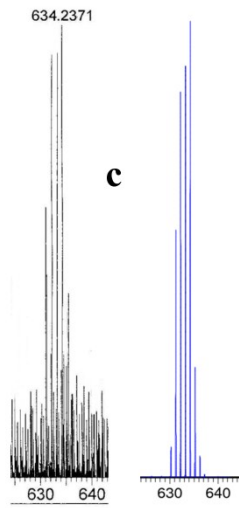
Experimental Simulated



b



Experimental Simulated



c

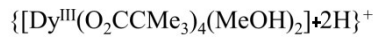


Figure S12. Experimental and simulated peaks obtained from HRMS (+ve) of **2** in MeOH corresponding to different species present in solution.

1 and **2** exhibits base peaks (Figures S11 and S13) due to the protonated ligands $\{\text{H}_2\text{L}1+\text{H}\}^+$ ($\text{C}_9\text{H}_{12}\text{NO}_2$; calcd, 166.0868) and $\{\text{H}_2\text{L}2+\text{H}\}^+$ ($\text{C}_{10}\text{H}_{14}\text{NO}_3$; calcd, 196.0974) at m/z =

166.0870 and 196.0972 respectively. A peak due the species $\{(CH_3)_3CCO_2H\}^+$ ($C_5H_{10}O_2$; calcd, 102.0681) appears at $m/z = 102.0669$ and 102.0662 in **1** and **2** respectively.

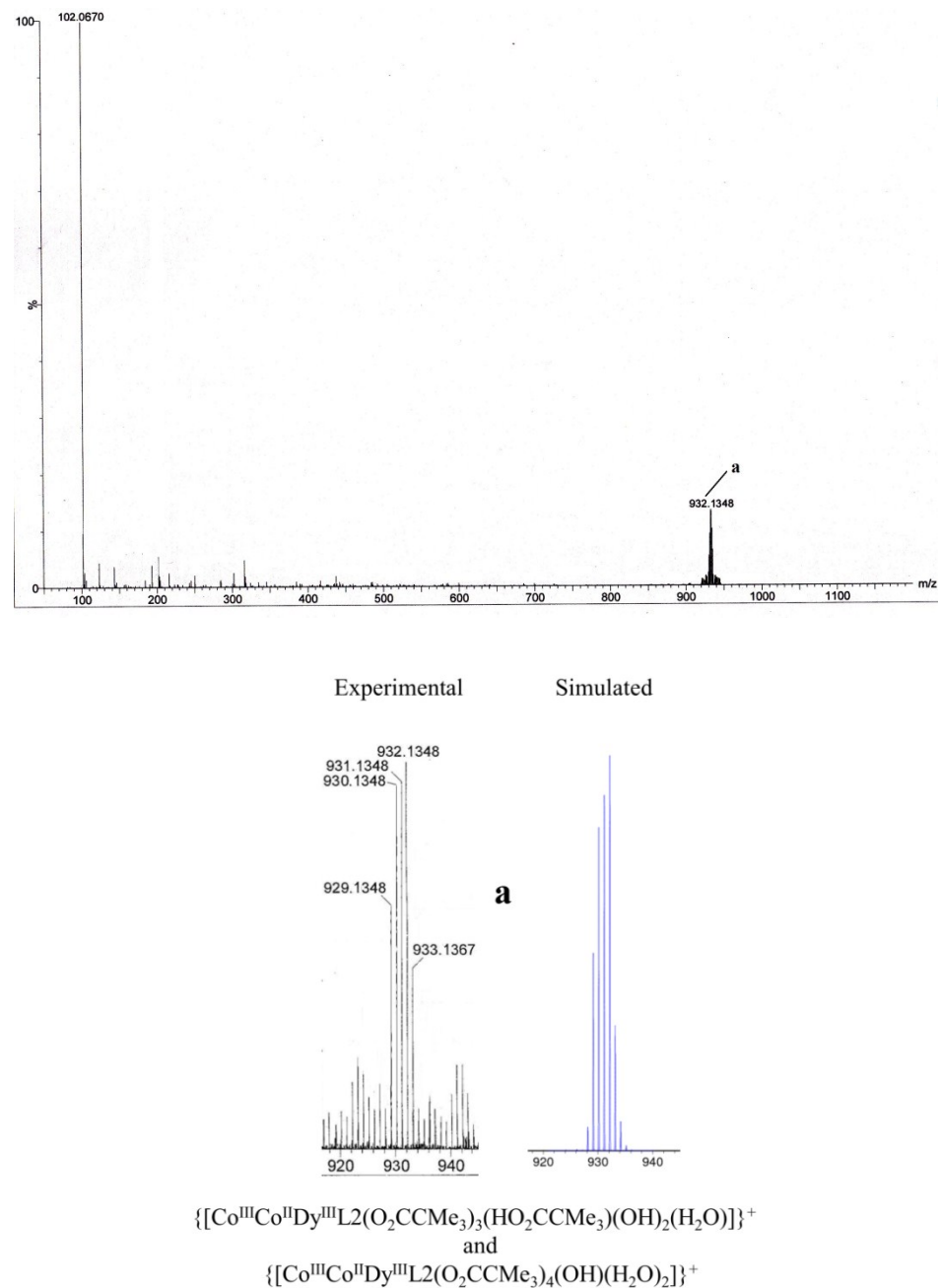


Figure S13. Experimental and simulated peaks obtained from HRMS (+ve) of **2** in MeCN corresponding to different species present in solution.

The base peak at $m/z = 102.0670$ is due to the species $\{(CH_3)_3CCO_2H\}^+$ ($C_5H_{10}O_2$; calcd, 102.0681).

Table S1. Important bond lengths (\AA) and angles ($^\circ$) in **1**, **2** and **3**

Bond lengths (\AA)					
Complex 1					
Dy1 – O4	2.369(7)	Dy3 – O17	2.384(11)	Co2 – O4	1.941(7)
Dy1 – O5	2.462(7)	Dy3 – O18	2.365(10)	Co2 – O5	1.943(7)
Dy1 – O15	2.339(6)	Dy3 – O19	2.284(12)	Co2 – O6	1.897(7)
Dy1 – O16	2.348(7)	Dy3 – O21	2.398(9)	Co2 – N1	1.875(9)
Dy2 – O3	2.417(8)	Co1 – O3	2.114(7)	Dy1 – Co1	3.4484(15)
Dy2 – O4	2.442(7)	Co1 – O5	2.115(7)	Dy1 – Co2	3.4604(13)
Dy2 – O7	2.341(8)	Co1 – O8	2.008(9)	Dy2 – Co1	3.4130(15)
Dy2 – O9	2.388(9)	Co1 – O10	2.131(9)	Dy2 – Co2	3.3850(15)
Dy2 – O12	2.294(9)	Co1 – O11	2.147(8)	Dy1 – Dy2	3.8802(2)
Dy2 – O13	2.408(9)	Co1 – O15	2.068(7)	Dy2 – Dy2	4.8284(4)
Dy2 – O14	2.347(9)	Co2 – O1	1.881(8)	Co1 – Co2	3.1099(3)
Dy2 – O15	2.361(6)	Co2 – O3	1.907(7)		
Complex 2					
Dy1 – O4	2.329(4)	Dy3 – O17	2.421(5)	Co2 – O5	1.950(4)
Dy1 – O5	2.491(4)	Dy3 – O18	2.375(5)	Co2 – O6	1.895(4)
Dy1 – O15	2.347(4)	Dy3 – O19	2.321(5)	Co2 – O15	1.928(4)
Dy1 – O16	2.352(4)	Dy3 – O21	2.357(5)	Co2 – N1	1.875(5)
Dy2 – O3	2.413(4)	Co1 – O3	2.139(4)	Dy1 – Co1	3.4667(9)
Dy2 – O4	2.384(4)	Co1 – O4	2.088(4)	Dy1 – Co2	3.4527(9)
Dy2 – O7	2.362(5)	Co1 – O5	2.120(4)	Dy2 – Co1	3.4297(10)
Dy2 – O9	2.367(5)	Co1 – O8	2.013(5)	Dy2 – Co2	3.3789(9)
Dy2 – O12	2.269(5)	Co1 – O10	2.103(5)	Dy1 – Dy2	3.8781(2)
Dy2 – O13	2.408(5)	Co1 – O11	2.201(5)	Dy2 – Dy2	4.8559(3)
Dy2 – O14	2.335(5)	Co2 – O1	1.888(4)	Co1 – Co2	3.1006(2)
Dy2 – O15	2.438(4)	Co2 – O3	1.904(4)		
Complex 3					
Dy1 – O1	2.386(2)	Co1 – O3	1.886(2)	Co2 – O12	2.158(2)
Dy1 – O2	2.598(3)	Co1 – O6	1.9264(19)	Co2 – O12	2.178(2)

Dy1 – O4	2.429(2)	Co1 – O11	1.907(2)	Dy1 – Co1	3.3986(5)
Dy1 – O5	2.399(2)	Co1 – O13	1.914(2)	Dy1 – Co2	3.8635(2)
Dy1 – O6	2.4126(19)	Co1 – N1	1.887(3)	Co1 – Co2	3.5895(2)
Dy1 – O7	2.233(2)	Co2 – O3	2.0047(19)	Co1 – Co2	3.4887(2)
Dy1 – O9	2.251(3)	Co2 – O6	2.1142(19)	Co2 – Co2	3.2213(1)
Dy1 – O14	2.323(2)	Co2 – O8	2.063(2)		
Co1 – O1	1.901(2)	Co2 – O10	2.094(2)		

Bond angles (°)

Complex 1

O15–Dy1–O15	104.3(3)	O14–Dy2–O13	77.5(4)	O6–Co2–O5	176.1(3)
O15–Dy1–O16	88.5(2)	O15–Dy2–O13	146.4(3)	O3–Co2–O5	83.9(3)
O15–Dy1–O16	142.6(2)	O9–Dy2–O13	68.1(4)	N1–Co2–O4	173.3(4)
O16–Dy1–O16	102.5(4)	O3–Dy2–O13	109.1(4)	O1–Co2–O4	92.2(3)
O15–Dy1–O4	78.4(2)	O12–Dy2–O4	75.8(3)	O6–Co2–O4	92.4(3)
O15–Dy1–O4	68.4(2)	O7–Dy2–O4	75.0(3)	O3–Co2–O4	87.2(3)
O16–Dy1–O4	80.4(2)	O14–Dy2–O4	128.6(3)	O5–Co2–O4	83.7(3)
O16–Dy1–O4	138.3(2)	O15–Dy2–O4	66.9(2)	O8–Co1–O15	96.6(4)
O4–Dy1–O4	124.9(3)	O9–Dy2–O4	134.1(3)	O8–Co1–O5	171.2(3)
O15–Dy1–O5	70.7(2)	O3–Dy2–O4	66.2(2)	O15–Co1–O5	83.3(3)
O15–Dy1–O5	142.3(2)	O13–Dy2–O4	145.7(3)	O8–Co1–O3	96.3(3)
O16–Dy1–O5	75.0(2)	O19–Dy3–O19	97.5(8)	O15–Co1–O3	84.0(3)
O16–Dy1–O5	77.8(2)	O19–Dy3–O18	156.2(4)	O5–Co1–O3	74.9(3)
O4–Dy1–O5	140.6(2)	O19–Dy3–O18	83.1(5)	O8–Co1–O10	87.1(4)
O4–Dy1–O5	64.9(2)	O18–Dy3–O18	105.9(7)	O15–Co1–O10	161.6(3)
O15–Dy1–O5	70.7(2)	O19–Dy3–O17	86.2(5)	O5–Co1–O10	95.8(3)
O4–Dy1–O5	64.9(2)	O19–Dy3–O17	151.3(4)	O3–Co1–O10	113.5(3)
O5–Dy1–O5	135.9(3)	O18–Dy3–O17	82.4(4)	O8–Co1–O11	89.6(4)
O12–Dy2–O7	79.8(3)	O18–Dy3–O17	52.4(3)	O15–Co1–O11	101.6(3)
O12–Dy2–O14	76.3(3)	O17–Dy3–O17	104.0(6)	O5–Co1–O11	99.0(3)
O7–Dy2–O14	139.1(3)	O19–Dy3–O21	79.1(4)	O3–Co1–O11	171.4(3)
O12–Dy2–O15	108.3(3)	O19–Dy3–O21	77.5(4)	O10–Co1–O11	60.4(3)

O7–Dy2–O15	137.0(3)	O18–Dy3–O21	77.8(4)	Co1–O15–Dy1	102.8(3)
O14–Dy2–O15	82.5(3)	O18–Dy3–O21	125.6(4)	Co1–O15–Dy2	100.6(3)
O12–Dy2–O9	148.0(3)	O17–Dy3–O21	75.3(4)	Dy1–O15–Dy2	111.3(3)
O7–Dy2–O9	115.0(3)	O17–Dy3–O21	129.2(4)	Co2–O4–Dy1	106.4(3)
O14–Dy2–O9	74.6(3)	O21–Dy3–O21	144.1(6)	Co2–O4–Dy2	100.5(3)
O15–Dy2–O9	80.8(3)	N1–Co2–O1	94.3(4)	Dy1–O4–Dy2	107.5(3)
O12–Dy2–O3	138.6(3)	N1–Co2–O6	86.1(4)	Co2–O3–Dy2	102.5(3)
O7–Dy2–O3	75.2(3)	O1–Co2–O6	87.0(3)	Co1–O3–Dy2	97.6(3)
O14–Dy2–O3	141.4(3)	N1–Co2–O3	86.5(4)	Co2–O3–Co1	101.2(3)
O15–Dy2–O3	71.7(2)	O1–Co2–O3	176.9(3)	Co2–O5–Dy1	102.9(3)
O9–Dy2–O3	73.3(3)	O6–Co2–O3	96.1(3)	Co1–O5–Dy1	97.5(2)
O12–Dy2–O13	92.9(4)	N1–Co2–O5	97.8(3)	Co2–O5–Co1	100.0(3)
O7–Dy2–O13	71.1(3)	O1–Co2–O5	93.0(3)		
Complex 2					
O4–Dy1–O4	111.8(2)	O14–Dy2–O13	79.94(18)	O6–Co2–O5	176.65(19)
O4–Dy1–O16	84.05(15)	O4–Dy2–O13	150.08(17)	O3–Co2–O5	85.23(18)
O4–Dy1–O16	144.44(16)	O9–Dy2–O13	71.14(18)	N1–Co2–O15	173.1(2)
O16–Dy1–O16	101.5(2)	O3–Dy2–O13	106.57(17)	O1–Co2–O15	91.34(18)
O4–Dy1–O15	78.67(15)	O12–Dy2–O15	74.10(15)	O6–Co2–O15	93.07(19)
O4–Dy1–O15	68.60(15)	O7–Dy2–O15	74.73(15)	O3–Co2–O15	87.29(18)
O16–Dy1–O15	136.51(15)	O14–Dy2–O15	129.80(16)	O5–Co2–O15	84.26(18)
O16–Dy1–O15	84.70(15)	O4–Dy2–O15	66.24(15)	O8–Co1–O4	95.65(19)
O15–Dy1–O15	120.0(2)	O9–Dy2–O15	133.22(15)	O8–Co1–O5	173.02(19)
O4–Dy1–O5	139.94(15)	O3–Dy2–O15	66.08(14)	O4–Co1–O5	83.51(16)
O4–Dy1–O5	70.99(14)	O13–Dy2–O15	141.95(17)	O8–Co1–O3	97.43(18)
O16–Dy1–O5	76.69(14)	O19–Dy3–O19	92.3(3)	O4–Co1–O3	84.13(17)
O16–Dy1–O5	74.60(14)	O19–Dy3–O18	152.1(2)	O5–Co1–O3	75.59(16)
O15–Dy1–O5	64.98(14)	O19–Dy3–O18	92.85(19)	O8–Co1–O10	86.9(2)
O15–Dy1–O5	144.60(14)	O18–Dy3–O18	95.3(3)	O4–Co1–O10	165.96(19)
O4–Dy1–O5	70.99(14)	O19–Dy3–O17	153.45(18)	O5–Co1–O10	95.57(18)
O4–Dy1–O5	139.94(15)	O19–Dy3–O17	81.01(19)	O3–Co1–O10	109.28(18)

O5–Dy1–O5	133.86(19)	O18–Dy3–O17	54.35(18)	O8–Co1–O11	88.19(19)
O12–Dy2–O7	78.97(17)	O18–Dy3–O17	82.24(19)	O4–Co1–O11	105.27(18)
O12–Dy2–O14	77.46(18)	O17–Dy3–O17	115.6(3)	O5–Co1–O11	98.72(17)
O7–Dy2–O14	137.80(17)	O19–Dy3–O21	77.92(18)	O3–Co1–O11	168.59(17)
O12–Dy2–O4	106.75(16)	O19–Dy3–O21	77.20(18)	O10–Co1–O11	60.94(19)
O7–Dy2–O4	136.54(15)	O18–Dy3–O21	129.89(18)	Co1–O4–Dy1	103.28(17)
O14–Dy2–O4	84.03(17)	O18–Dy3–O21	77.15(19)	Co1–O4–Dy2	99.95(18)
O12–Dy2–O9	149.87(17)	O17–Dy3–O21	75.54(17)	Dy1–O4–Dy2	110.71(17)
O7–Dy2–O9	116.54(18)	O17–Dy3–O21	125.51(17)	Co2–O15–Dy1	107.31(18)
O14–Dy2–O9	74.17(18)	O21–Dy3–O21	143.8(3)	Co2–O15–Dy2	100.75(18)
O4–Dy2–O9	80.28(16)	N1–Co2–O1	95.5(2)	Dy1–O15–Dy2	108.26(17)
O12–Dy2–O3	136.74(16)	N1–Co2–O6	86.2(2)	Co2–O3–Dy2	102.36(18)
O7–Dy2–O3	75.00(15)	O1–Co2–O6	86.3(2)	Co1–O3–Dy2	97.60(17)
O14–Dy2–O3	142.44(17)	N1–Co2–O3	85.9(2)	Co2–O3–Co1	100.00(18)
O4–Dy2–O3	72.35(14)	O1–Co2–O3	177.3(2)	Co2–O5–Dy1	101.35(17)
O9–Dy2–O3	73.38(15)	O6–Co2–O3	96.67(19)	Co1–O5–Dy1	97.17(16)
O12–Dy2–O13	94.24(18)	N1–Co2–O5	96.6(2)	Co2–O5–Co1	99.17(18)
O7–Dy2–O13	67.46(17)	O1–Co2–O5	92.28(18)		

Complex 3

O7–Dy1–O9	93.75(10)	O9–Dy1–O2	157.37(9)	O3–Co2–O10	90.54(9)
O7–Dy1–O14	152.08(8)	O14–Dy1–O2	96.04(9)	O8–Co2–O10	91.31(10)
O9–Dy1–O14	93.59(10)	O1–Dy1–O2	61.44(8)	O3–Co2–O6	165.94(8)
O7–Dy1–O1	83.16(8)	O5–Dy1–O2	75.96(9)	O8–Co2–O6	102.05(8)
O9–Dy1–O1	141.15(8)	O6–Dy1–2	126.18(8)	O10–Co2–O6	93.23(8)
O14–Dy1–O1	74.33(8)	O4–Dy1–O2	78.64(10)	O3–Co2–O12	88.59(8)
O7–Dy1–O5	76.07(9)	O3–Co1–N1	86.64(10)	O8–Co2–O12	92.80(9)
O9–Dy1–O5	82.34(10)	O3–Co1–O1	178.30(10)	O10–Co2–O12	175.82(9)
O14–Dy1–O5	131.65(8)	N1–Co1–O1	94.38(11)	O6–Co2–O12	86.67(8)
O1–Dy1–O5	133.22(9)	O3–Co1–O11	93.55(9)	O3–Co2–O12	87.14(8)
O7–Dy1–O6	79.03(8)	N1–Co1–O11	86.94(11)	O8–Co2–O12	176.55(9)
O9–Dy1–O6	76.01(8)	O1–Co1–O11	87.87(9)	O10–Co2–O12	91.82(9)

O14–Dy1–O6	76.70(7)	O3–Co1–O13	88.41(9)	O6–Co2–O12	79.21(8)
O1–Dy1–O6	65.35(7)	N1–Co1–O13	86.84(11)	O12–Co2–O12	84.05(8)
O5–Dy1–O6	145.63(8)	O1–Co1–O13	90.29(9)	Co1–O1–Dy1	104.30(9)
O7–Dy1–O4	129.41(9)	O11–Co1–O13	173.35(9)	Co1–O3–Co2	127.46(11)
O9–Dy1–O4	83.37(10)	O3–Co1–O6	93.74(8)	Co1–O6–Co2	125.27(10)
O14–Dy1–O4	78.23(8)	N1–Co1–O6	178.96(10)	Co1–O6–Dy1	102.54(8)
O1–Dy1–O4	127.77(8)	O1–Co1–O6	85.22(9)	Co2–O6–Dy1	117.03(8)
O5–Dy1–O4	53.43(8)	O11–Co1–O6	94.00(9)	Co2–O12–Co2	95.95(8)
O6–Dy1–O4	146.21(8)	O13–Co1–O6	92.21(9)		
O7–Dy1–O2	87.24(9)	O3–Co2–O8	91.38(9)		

Table S2 Continuous Shape Measures calculation for Dy^{III} in **1**, **2** and **3**

Complex	Metal ion center	Structure	
		Square Antiprism	Triangular Dodecahedron
1	Dy1	1.729	<u>1.034</u>
	Dy2	<u>0.989</u>	1.680
	Dy3	3.750	<u>2.841</u>
2	Dy1	<u>1.369</u>	1.953
	Dy2	<u>1.200</u>	1.496
	Dy3	4.253	<u>1.765</u>
3	Dy1	4.185	<u>2.339</u>

Table S3 Continuous Shape Measures calculation for Co^{II} and Co^{III} in **1**, **2** and **3**

Complex	Metal ion center	Octahedron
1	Co1	2.922
	Co2	0.364
2	Co1	2.819
	Co2	0.371
3	Co1	0.208
	Co2	0.427

Table S4. Hydrogen bonding parameters for **1–2**

Interactions	Type of H-bond	D–H (Å)	D···A (Å)	H···A (Å)	D–H···A (Å)
Complex 1					
O4–H4···O22	Inter	0.86(13)	3.18(3)	2.39(13)	153(10)
O15–H15···O22	Inter	0.98	3.18(3)	2.30	149
O16–H16A···O11	Intra	0.91	2.719(11)	1.82	170
O16–H16B···O1	Intra	0.91	2.587(11)	1.74	155
O13–H13B···O23	Inter	1.05	2.95(4)	2.56	101
O23···O20	Inter	—	2.7645(2)	—	—
O21–H21···O20	Intra	0.85(8)	2.648(18)	1.99(17)	135(16)
Complex 2					
O15–H15···O22	Inter	0.97(4)	2.785(7)	1.82(4)	172(7)
O22–H22···O1	Inter	0.82	3.115(7)	2.37	136
O16–H16F···O1	Intra	0.93	2.6423(1)	2.546	85
O16–H16E···O11	Intra	0.93	2.735(8)	1.96	140
O13–H13···O23	Inter	0.93	2.714(10)	1.98	134
O23–H23···O20	Inter	0.82	2.705(9)	1.92	161
O21–H21···O20	Intra	0.93	2.615(7)	2.00	122

Calculation of local electronic structure of metal ions and the magnetic properties of 1–2

Computational Details :

We have constituted model fragments containing one single magnetic center by substituting remaining center with diamagnetic ions. As complexes **1–2** contain total six paramagnetic centers (four Dy^{III} and two Co^{II}), we have performed calculations on six individual magnetic fragments comprising one paramagnetic centers only while other being substituted by diamagnetic ions. All other atoms (including diamagnetic Co^{III}) were retained as in the crystal structure, and we have not performed any geometry optimization.

Basis Sets :

All employed basis sets were taken from the standard ANO-RCC basis set library from MOLCAS 8.0. The following contractions were used for the atoms:

Dy: 8s7p5d3f2g1h.

Co: 6s5p3d2f1g.

Zn: 5s4p2d.

Lu: 7s6p4d2f.

C: 3s2p.

N: 3s2p1d.

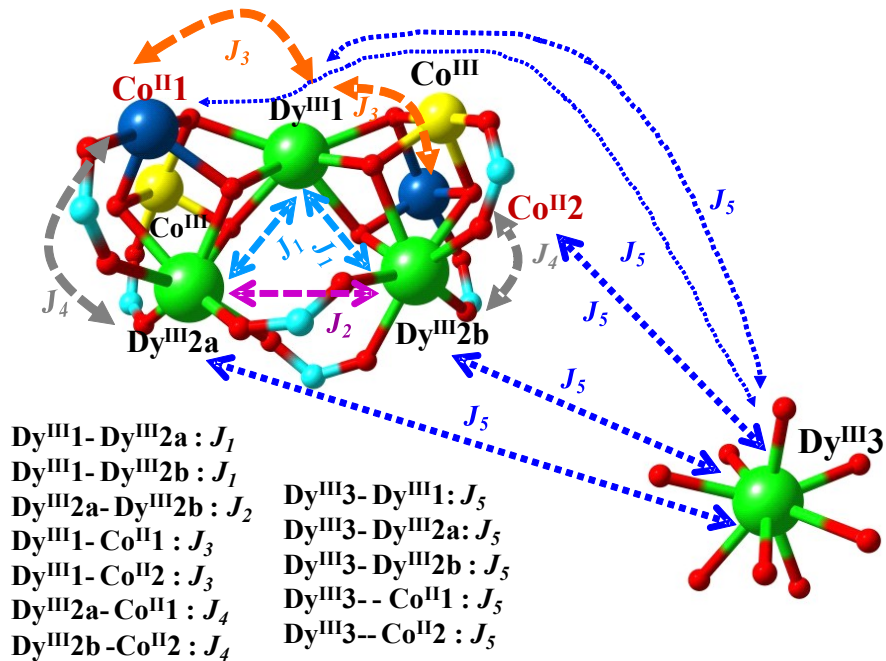
H: 2s.

O: 3s2p1d.

The active space of the Complete Active Space Self-Consistent-Field (CASSCF) method^{R1} for Co^{II} fragments incorporated 7 electrons spanning the five 3d orbitals. For Ln^{III} fragments, the active space comprised the nine electrons in seven 4f orbitals. The dynamic correlation (CASPT2) was not considered either for Co^{II} or Ln^{III} fragment.

For **Co fragments**, the active space of the CASSCF method included 7 electrons in 5 (3d) orbitals. The spin orbit interaction was computed by mixing of 10 quartets and 40 doublet spin free states.

For **Ln fragments** the active space of the CASSCF method incorporated all nine electrons from the last shell electrons in 7 orbitals of the 4f type. With this active space, 21 sextets were computed within configuration interaction (CI) procedure. Subsequently, spin-orbit interaction was estimated by mixing these 21 sextets within RASSI-SO approach.



Scheme S2. Core structural motif utilized for the estimation of different magnetic exchange interactions (J_1 - J_5).

The spin terms acquired in the CASSCF calculations were further mixed by the spin-orbit coupling within the Restricted Active Space State Interaction (RASSI-SO) approach.^{R2} The

acquired spin-orbit multiplets were consequently harnessed by the SINGLE_ANISO module^{R3} to deduce the D and g tensors, orientation of main magnetic axis and main anisotropy axis, and local magnetic properties^{R4}, which represents magnetic interaction between the spin moments of magnetic centers in absence of spin-orbit coupling by one parameter.^{R5} Within this model, the following effective Heisenberg Hamiltonian (Eq. (1))^{R6} is considered.

$$\hat{H}_{ex} = - \sum_{i=1}^3 J_i S_i \cdot S_{i+1} \cdots (1)$$

Here, $J_i = J_i^{dipolar} + J_i^{exch}$; i.e. J_i is the total magnetic interaction in combination of calculated $J_i^{dipolar}$ and fitted J_i^{exch} parameters; this summation depicts interaction between the Dy^{III} centres and Dy^{III}-Co^{II} sites. This exchange Hamiltonian corresponds to the local S=5/2 and S=3/2 spins on Dy^{III} and Co^{II} centres respectively in the absence of spin-orbit coupling and has been diagonalized based on the KDS acquired from fragment *ab initio* calculations.

Table S5. Energies (cm⁻¹) of the spin-free (CASSCF) and spin-orbit (RASSI) states of the individual magnetic centers in Complex 1

Spin multiplicity	Spin free states (CASSCF)						Spin-orbit states (RASSI)					
	Dy1	Dy2a	Dy2b	Dy3	Co1	Co2	Dy1	Dy2a	Dy2b	Dy3	Co1	Co2
6	0	0	0	0			0	0	0	0	0	0
	1.382	11.753	11.751	10.059			112.611	56.557	56.564	14.171	164.411	165.126
	59.052	79.409	79.416	65.017			125.142	90.414	90.419	69.571	833.856	842.254
	66.806	90.407	90.411	147.381			154.94	145.569	145.575	120.448	1099.044	1201.827
	121.284	142.129	142.133	151.144			189.14	219.93	219.937	141.51	1900.072	1934.78
	162.998	266.578	266.579	168.244			212.754	306.893	306.899	218.516	2012.934	2135.367
	213.745	311.829	311.831	250.759			368.371	384.573	384.581	280.253	6990.118	7341.289
	381.57	426.729	426.73	341.183			490.97	491.004	491.01	294.008	7048.234	7356.963
	383.05	438.39	438.394	393.084			3028.493	3015.386	3015.39	3054.963	7184.894	7432.157
	499.93	546.207	546.21	401.154			3071.318	3067.082	3067.09	3068.995	7236.249	7393.979
	501.367	558.244	558.248	514.17			3136.488	3122.641	3122.646	3088.831	8001.141	8089.121
	7515.646	7579.861	7579.867	7549.178			3180.684	3174.759	3174.765	3105.96	8106.663	8234.359
	7585.597	7598.821	7598.826	7569.985			3226.551	3237.543	3237.55	3120.663	14619.66	14657.19
	7622.756	7702.501	7702.506	7603.464			3260.078	3305.624	3305.632	3169.608	14625.44	14683.45
	7666.046	7733.401	7733.404	7699.381			3327.857	3352.99	3352.999	3180.731	14735.27	14791.27
	7750.131	7772.489	7772.494	7749.103			5630.323	5612.739	5612.746	5601.115	16673.98	16953.20
	7770.887	7815.394	7815.399	7767.808			5656.299	5666.817	5666.824	5647.271	19961.39	19984.36
	7789.933	7837.913	7837.917	7798.657			5740.922	5726.11	5726.117	5682.093	20251.92	20318.25
	34720.58	34769.38	34769.39	34940.71			5789.292	5786.47	5786.477	5701.12	20749.29	20942.33
	35048.66	35019.43	35019.44	34983.39			5832.823	5829.908	5829.918	5718.995	21316.51	21452.67
	35131.15	35296.72	35296.74	34994.96			5834.284	5903.74	5903.75	5750.432	21619.53	21734.87
4				0	0	7818.67	7803.978	7803.986	7773.893	21872.56	22014.25	
				623.142	623.263	7856.331	7862.963	7862.971	7820.906	23048.48	23146.89	
				1636.032	1639.015	7935.738	7936.018	7936.026	7870.238	23122.59	23486.14	
				6710.065	6714.118	7988.41	7977.977	7977.988	7894.787	24265.52	24361.96	
				6899.436	6906.598	8010.757	8065.894	8065.904	7924.533	24397.58	24428.54	
				7723.923	7741.571	9557.694	9555.194	9555.202	9495.423	25272.44	25334.61	
				14276.7	14294.3	9576.042	9570.231	9570.24	9513.825	25445.62	25572.29	
				22897.59	22914.67	9587.017	9603.21	9603.218	9540.015	25813.16	25937.36	
				24158.12	24173.45	9632.429	9627.518	9627.527	9564.207	26210.18	26347.72	
				25622.29	25678.50	9655.471	9669.951	9669.96	9579.844	26679.61	26845.90	
2				14448.24	14479.56	9670.884	9681.246	9681.255	9596.33	27137.76	27694.25	

				16395.73	16405.82	9688.14	9699.166	9699.175	9647.955	29188.91	29393.81
				19758.18	19797.39	9710.426	9726.829	9726.838	9664.207	29537.61	29658.38
				19925.18	19953.41	9777.121	9768.623	9768.632	9687.606	29898.39	29989.45
				20558.69	20571.23	9799.891	9854.847	9854.858	9733.368	30131.06	30256.12
				20911.12	20957.34	10948.09	10945.57	10945.58	10962.7	30552.26	30678.73
				21209.64	21242.79	11121.95	11116.51	11116.52	11033.03	30851.81	30895.34
				21451.52	21499.22	11214.78	11248.71	11248.72	11080.79	31972.31	31990.26
				25205.28	25248.67	11771.4	11784.35	11784.36	11707.3	32502.73	32784.09
				25319.33	25365.70	11792.33	11803.5	11803.51	11747.16	34258.06	34367.95
				26192.84	26225.12	11833.14	11834.88	11834.89	11756.88	34840.52	34923.64
				26394.5	26467.25	11852.72	11867.24	11867.25	11785.02	35249.34	35375.81
				28870.32	28914.32	11859.15	11879.45	11879.46	11809.74	35630.47	35819.50
				29167.32	29232.56	13543.77	13559.63	13559.65	13472.12	36132.77	36482.90
				29569.22	29671.48	13569.28	13584.93	13584.94	13511.77	36273.6	36381.23
				29736.76	29824.13	13634.1	13642.84	13642.85	13576.75	36570.58	36728.19
				30241.84	30325.80	13652.77	13661.53	13661.54	13588.13	37123.54	37465.44
				30514.96	30593.61	14950.54	14967.24	14967.25	14880.68	46864.84	46927.22
				31624.54	31782.54	14978.82	14990.41	14990.42	14924.56	47362.83	47480.56
				32111.31	32243.69	15021.49	15031.43	15031.44	14954.11	47940.38	48013.77
				34032.3	34165.28	15974	15982.77	15982.78	15910.39	48335.5	48432.59
				34624.69	34783.47	15980.28	15995.48	15995.5	15914.36	48711.01	48920.15
				35072.44	35193.52	16570.12	16583.68	16583.7	16503.57	49344.08	49444.30
				35166.04	35241.27	38807.01	38793.63	38793.64	38839.77	49598.77	49832.27
				35527.05	35628.01	38846.26	38875.43	38875.44	38846.09	71366.75	711369.58
				35987.23	36413.59	38911.35	38943.11	38943.13	38855.07	71768.16	71902.73
				36108.75	36257.69	39038.59	39065.41	39065.43	38869.43	73259.53	73467.18
				36462.46	36813.78	40180.49	40185.6	40185.61	40219.39	73876.34	73990.38
				46622.49	46752.49	40326.22	40319.95	40319.97	40240.51	74219.65	74365.48
				47016.98	47613.27	40420.34	40503.76	40503.79	40252.97		
				47603.37	47735.20	41279.32	41309.57	41309.59	41223.6		
				47989.67	48214.60	41329.69	41367.84	41367.86	41230.04		
				48412.71	48728.25						
				48973.58	49115.32						
				49245.42	49547.17						
				71043.95	71567.36						
				71408.77	71526.24						
				72933.12	73135.68						

Table S6. Energies (cm^{-1}) of the lowest Kramers doublets on individual magnetic centers in 1

Dy1	Dy2a	Dy2b	Dy3	Co1	Co2
0	0	0	0	0	0
112.611	56.557	56.564	14.171	164.411	165.126
125.142	90.414	90.419	69.571	833.856	842.254
154.94	145.569	145.575	120.448	1099.044	1201.827
189.14	219.93	219.937	141.51	1900.072	1934.78
212.754	306.893	306.899	218.516	2012.934	2135.367
368.371	384.573	384.581	280.253		
490.97	491.004	491.01	294.008		
Main values of the g tensor of lowest Kramers doublets					
$g_x=0.02$	$g_x=0.05$	$g_x=0.05$	$g_x=10.99$	$g_x=1.48$	$g_x=1.43$
$g_y=0.03$	$g_y=0.06$	$g_y=0.06$	$g_y=7.13$	$g_y=2.09$	$g_y=1.98$
$g_z=19.92$	$g_z=19.23$	$g_z=19.22$	$g_z=1.36$	$g_z=8.02$	$g_z=8.08$
Unquenched orbital moment $\langle L_z \rangle$ in the ground state doublet (μ_B)					
4.96	4.79	4.79	0.34	1.26	1.28
Alignment of first excited KD main anisotropy axis with respect to that of ground KD (in °)					
0.34*	109.32	109.32	169.02	90.68	90.75
Zero-field splitting parameters (cm^{-1}) of Co ^{II} site assuming pseudospin $\tilde{S}=3/2$					
Co1 site : D= -73.33, {D _x = 45.89, D _y =3.00, D _z = -48.89}, E = 21.45					
Co2 site : D= -93.46, {D _x = 50.82, D _y =11.48, D _z = -62.30}, E = 19.67					
Values of g tensor of Co ^{II} site assuming $\tilde{S}=3/2$					
Co1 site : $g_x=2.00$, $g_y=2.36$, $g_z=2.94$					
Co2 site : $g_x=2.00$, $g_y=2.35$, $g_z=2.94$					

* Due to small deviation, relaxation occurs via second excited KD, in which main anisotropy axis forms an angle of 90.05° with respect to ground KD.

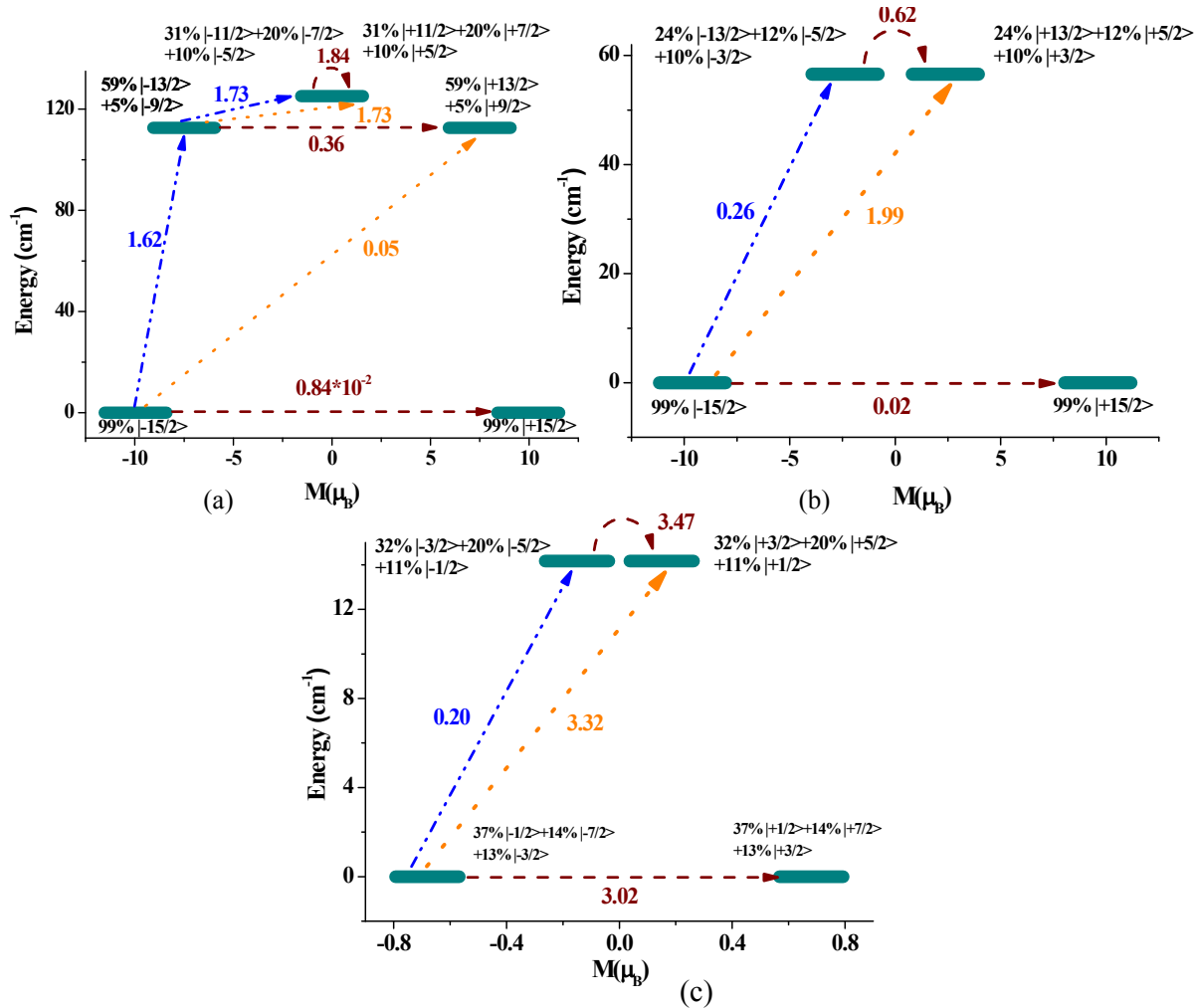


Figure S14. Ab initio computed Single-Ion based magnetization relaxation blockade for (a) Dy1, (b) Dy2a (similar mechanism observed for Dy2b site) and (c) Dy3 sites respectively in complex **1**.

Table S7. *Ab initio* computed crystal field parameters in complex **1** for different magnetic centres

k	q	B_k^q	B_k^q	B_k^q	B_k^q
		Dy1	Dy2a	Dy2b	Dy3
2	-2	2.43E-03	2.40E+00	-2.39E+00	-3.53E-03
	-1	1.52E+00	-1.59E+00	-1.56E+00	1.07E-02
	0	-1.76E+00	-1.63E+00	-1.63E+00	-5.69E-02
	1	-8.14E-03	2.22E+00	-2.24E+00	6.91E-01
	2	7.24E-01	-3.02E-01	-3.73E-01	-8.98E-02
4	-4	2.74E-04	-1.36E-02	1.17E-02	2.84E-03
	-3	-2.82E-02	6.31E-02	6.43E-02	1.88E-03
	-2	-1.64E-05	-3.09E-03	3.23E-03	3.29E-05
	-1	-1.14E-02	1.77E-02	1.76E-02	2.40E-05
	0	-4.07E-04	-2.12E-03	-2.12E-03	-1.28E-03
	1	-7.06E-06	-4.26E-03	4.50E-03	-2.14E-03

	2	-1.42E-02	-3.23E-03	-3.15E-03	3.26E-03
	3	-3.84E-05	3.04E-02	-2.74E-02	4.97E-02
	4	4.80E-02	3.19E-02	3.27E-02	4.97E-02
6	-6	1.20E-06	3.58E-05	-4.11E-05	-3.13E-06
	-5	2.01E-04	-1.00E-03	-1.01E-03	1.19E-05
	-4	3.08E-07	-1.38E-04	1.36E-04	-3.83E-06
	-3	8.79E-05	-2.15E-04	-2.15E-04	1.55E-05
	-2	5.23E-07	2.34E-05	-2.54E-05	-4.39E-06
	-1	4.13E-05	-1.79E-04	-1.79E-04	4.75E-06
	0	-1.70E-05	2.82E-06	2.98E-06	2.20E-05
	1	-8.05E-07	-1.04E-04	1.00E-04	3.30E-04
	2	1.81E-04	8.92E-05	8.89E-05	-1.31E-04
	3	5.11E-07	-1.01E-04	9.31E-05	3.15E-04
	4	-1.02E-04	1.47E-05	2.35E-05	-4.52E-05
	5	-3.19E-07	-2.13E-04	1.38E-04	1.92E-04
	6	1.36E-04	5.99E-05	5.63E-05	-4.23E-05

Table S8. Energies (cm⁻¹) of the spin-free (CASSCF) and spin-orbit (RASSI) states of the individual magnetic centers in Complex 2

Spin multiplicity	Spin free states (CASSCF)						Spin-orbit states (RASSI)					
	Dy1	Dy2a	Dy2b	Dy3	Co1	Co2	Dy1	Dy2a	Dy2b	Dy3	Co1	Co2
6	0	0	0	0			0	0	0	0	0	0
	4.398	27.413	33.192	17.797			101.049	25.44	39.552	13.586	165.005	164.29
	49.03	60.977	70	45.727			114.469	81.515	92.747	32.508	831.629	831.579
	53.039	120.907	128.668	120.08			140.45	137.396	146.64	67.967	1102.705	1102.582
	135.128	161.987	168.015	145.032			189.319	187.136	195.75	86.122	1761.32	1757.637
	140.889	254.884	271.129	179.071			198.077	254.952	280.007	166.639	1878.253	1875.255
	198.347	279.82	306.805	215.987			322.674	310.772	316.966	202.549	6514.308	6494.238
	341.52	373.577	380.472	242.227			528.437	449.523	458.456	363.958	6598.963	6579.635
	348.49	382.079	390.486	320.85			3024.274	3010.404	3013.931	2998.527	7332.246	7334.798
	543.331	520.155	530.574	474.515			3060.619	3048.126	3064.075	3039.581	7393.979	7396.486
	543.899	526.601	539.039	504.41			3120.872	3094.991	3108.416	3045.842	7681.979	7689.453
	7500.752	7571.579	7578.932	7540.233			3160.754	3141.663	3151.461	3077.339	7814.437	7822.337
	7585.246	7595.238	7606.378	7571.27			3219.979	3203.227	3212.362	3093.931	14278.09	14277.14
	7642.232	7690.438	7698.938	7607.336			3243.843	3252.368	3265.703	3137.177	14284.65	14283.6
	7657.245	7726.64	7740.213	7645.63			3352.13	3308.785	3317.249	3217.567	14791.43	14778.53
	7750.014	7755.283	7760.463	7718.061			5613.467	5604.45	5610.995	5573.991	16872.71	16887.07
	7775.438	7789.92	7801.803	7766.489			5653.502	5646.938	5662.297	5605.745	19946.15	19939.45
	7779.954	7804.814	7819.305	7782.412			5721.66	5691.902	5699.677	5634.918	20215.28	20202.55
	34719.25	34809.21	34814.067	34860.14			5764.697	5747.429	5758.103	5661.68	20612.88	20602.98
	35006.79	34983.35	35000.81	34924.1			5832.088	5791.432	5803.757	5723.403	21213.31	21221.41
	35176.38	35265.07	35272.461	35112.95			5856.722	5860.608	5870.617	5752.208	21599.54	21590.39
4					0	0	7800.431	7795.077	7802.501	7754.743	21878.15	21878.72
					626.179	626.127	7851.006	7837.089	7849.328	7786.739	22908.17	22952.32
					1483.594	1480.122	7913.808	7897.843	7907.141	7814.334	22974.82	23017.21
					6227.628	6207.461	7994.051	7940.183	7952.462	7887.885	23963.13	23892.34
					7080.404	7083.314	8015.265	8026.709	8037.009	7921.852	24093.49	24024.73
					7388.936	7396.859	9549.632	9530.988	9542.81	9470.134	25147.64	25150.41
					13925.58	13924.65	9564.588	9556.313	9563.125	9498.859	25360.86	25370.82
					22746.26	22792.42	9580.48	9583.851	9590.853	9515.483	25791.79	25808.23
					23834.87	23760.65	9611.516	9596.694	9607.142	9533.028	26208.47	26225.66
					25608.83	25630.37	9642.155	9636.405	9646.648	9554.804	26597.93	26592.42
2					14503.83	14490.97	9660.077	9649.622	9659.561	9581.964	26944.32	26926.27
					16592.43	16607.04	9683.071	9659.772	9673.05	9596.219	29160.73	29170.86

					19761.99	19751.45	9718.982	9692.541	9706.653	9639.488	29445.18	29436.85
					19871.11	19862.41	9783.292	9729.774	9740.977	9673.738	29692.45	29696.81
					20369.86	20351.63	9802.657	9812.677	9824.367	9715.96	29912.23	29910.3
					20797.92	20814.81	10941.28	10933.92	10944.383	10915.94	30388.14	30406
					21252.6	21245.46	11089.22	11078.95	11089.359	10986.03	30799.27	30795.2
					21420.85	21418.75	11233.84	11204.29	11214.3	11107.32	31789.04	31810.46
					24991.81	24987.84	11758.45	11754.9	11765.846	11678.81	32317.13	32294.69
					25336.06	25358.61	11795.2	11780.13	11790.805	11727.69	34108.81	34116.96
					26095.57	26054.63	11829.13	11803.03	11813.065	11741.66	34588	34589.2
					26210.58	26216.56	11847.75	11826.88	11838.323	11750.35	35038.65	35021.79
					28878.69	28900.73	11854.37	11844.9	11857.323	11778.9	35302.95	35308.61
					29068.47	29054.07	13535.55	13531.6	13540.734	13461.73	35831.97	35827.96
					29360.81	29364.27	13567.72	13557.13	13569.193	13479.86	35940.63	35942.16
					29462.1	29454.23	13630.78	13608.51	13619.127	13546.88	36242.12	36239.78
					30065.33	30086.15	13645.52	13626.28	13637.974	13562.56	36843.33	36829.43
					30471.83	30467	14947.19	14937.78	14947.648	14861.77	46742.45	46738.46
					31431.3	31454.69	14971.3	14960.14	14971.599	14898.36	47312.24	47313.32
					31917.85	31892.81	15017.06	14997.92	15008.936	14928.5	47753.55	47738.95
					33892.39	33902.37	15966.7	15951.98	15962.74	15884.37	48283.61	48305.56
					34367.79	34366.27	15977.06	15963.4	15974.233	15893.14	48574.75	48563.88
					34834.97	34814.94	16565.42	16551.83	16562.608	16481.3	49205.99	49207.32
					34970.29	34966.7	38789.85	38785.3	38796.054	38761.41	49428.14	49428.13
					35111.55	35129.91	38847.93	38866.58	38875.549	38816.71	71159.12	71168.09
					35624.98	35622.68	38910.64	38927.62	38936.127	38855.53	71597.64	71603.34
					35738.12	35734.91	39035.01	39016.65	39029.579	38891.52	73209.5	73214.41

Table S9. Energies (cm^{-1}) of the lowest Kramers doublets on individual magnetic centers in **2**

Dy1	Dy2a	Dy2b	Dy3	Co1	Co2
0	0	0	0	0	0
101.049	25.44	39.552	13.586	165.005	164.29
114.469	81.515	92.747	32.508	831.629	831.579
140.45	137.396	146.64	67.967	1102.705	1102.582
189.319	187.136	195.75	86.122	1761.32	1757.637
198.077	254.952	280.007	166.639	1878.253	1875.255
322.674	310.772	316.966	202.549		
528.437	449.523	458.456	363.958		
Main values of the g tensor of lowest Kramers doublets					
$g_x = 0.03$	$g_x = 1.12$	$g_x = 0.62$	$g_x = 3.67$	$g_x = 1.61$	$g_x = 1.63$
$g_y = 0.07$	$g_y = 4.48$	$g_y = 1.69$	$g_y = 5.32$	$g_y = 2.34$	$g_y = 2.45$
$g_z = 19.87$	$g_z = 16.00$	$g_z = 18.50$	$g_z = 10.40$	$g_z = 7.86$	$g_z = 7.81$
Unquenched orbital moment $\langle L_z \rangle$ in the ground state doublet (μ_B)					
4.95	3.98	4.60	2.58	1.24	1.23
Alignment of first excited KD main anisotropy axis with respect to that of ground KD (in °)					
69.77	78.02	67.62	6.00	90.44	90.47
Zero-field splitting parameters (cm^{-1}) of Co ^{II} site assuming pseudospin $\tilde{S} = 3/2$					
Co1 site : D= 71.53, {D _x = 47.69, D _y = -0.11, D _z = -47.58}, E = 23.74					
Co2 site : D= 71.69, {D _x = 47.79, D _y = -0.74, D _z = -47.05}, E = 23.16					
Values of g tensor of Co ^{II} site assuming $\tilde{S} = 3/2$					
Co1 site : $g_x = 2.00$, $g_y = 2.40$, $g_z = 2.93$					
Co2 site : $g_x = 2.00$, $g_y = 2.41$, $g_z = 2.93$					

Table S10. *Ab initio* computed crystal field paramaters in complex **2** for different magnetic centres

k	q	B_k^q	B_k^q	B_k^q	B_k^q
		Dy1	Dy2	Dy3	Dy4
2	-2	-8.57E-01	-1.55E-01	2.57E-01	-7.84E-03
	-1	-1.70E+00	2.49E+00	-2.53E+00	-1.13E-02
	0	-1.72E+00	-7.82E-01	-1.02E+00	2.94E-01
	1	-1.04E+00	2.16E+00	2.21E+00	3.63E+00
	2	1.15E+00	2.71E+00	2.44E+00	3.72E-01
4	-4	-4.39E-02	3.86E-03	-4.06E-03	-1.64E-04
	-3	-4.07E-03	6.42E-02	-6.59E-02	-1.09E-03
	-2	1.40E-02	1.21E-02	-1.09E-02	-2.87E-04
	-1	1.01E-02	2.02E-03	1.51E-03	-4.62E-04
	0	1.24E-04	-4.67E-03	-4.79E-03	2.14E-03
	1	2.54E-03	3.61E-04	-7.21E-03	4.38E-04
	2	-1.07E-02	1.20E-02	8.80E-03	2.90E-02
	3	2.46E-02	-1.56E-03	-6.02E-03	6.59E-02
	4	-1.26E-02	-1.38E-02	-1.75E-02	1.16E-02
6	-6	-8.82E-05	3.10E-05	-4.58E-05	8.90E-07
	-5	8.46E-05	4.39E-04	-4.86E-04	1.48E-06

	-4	7.44E-05	1.68E-04	-1.65E-04	-2.64E-06
	-3	2.26E-05	3.07E-04	-2.35E-04	-3.18E-06
	-2	-1.54E-04	3.23E-06	1.74E-05	-2.32E-06
	-1	9.15E-06	-1.33E-04	1.44E-04	4.22E-06
	0	-2.27E-05	6.78E-06	1.25E-05	3.76E-07
	1	6.54E-05	-3.59E-05	1.17E-07	-2.03E-04
	2	1.21E-04	-6.42E-05	-7.38E-05	-1.63E-04
	3	-7.33E-05	1.17E-04	5.58E-05	5.25E-04
	4	1.71E-05	-2.83E-05	-6.81E-05	3.54E-05
	5	-1.98E-04	-4.09E-04	-6.37E-04	-3.53E-04
	6	-2.01E-04	1.14E-04	1.14E-04	5.27E-06

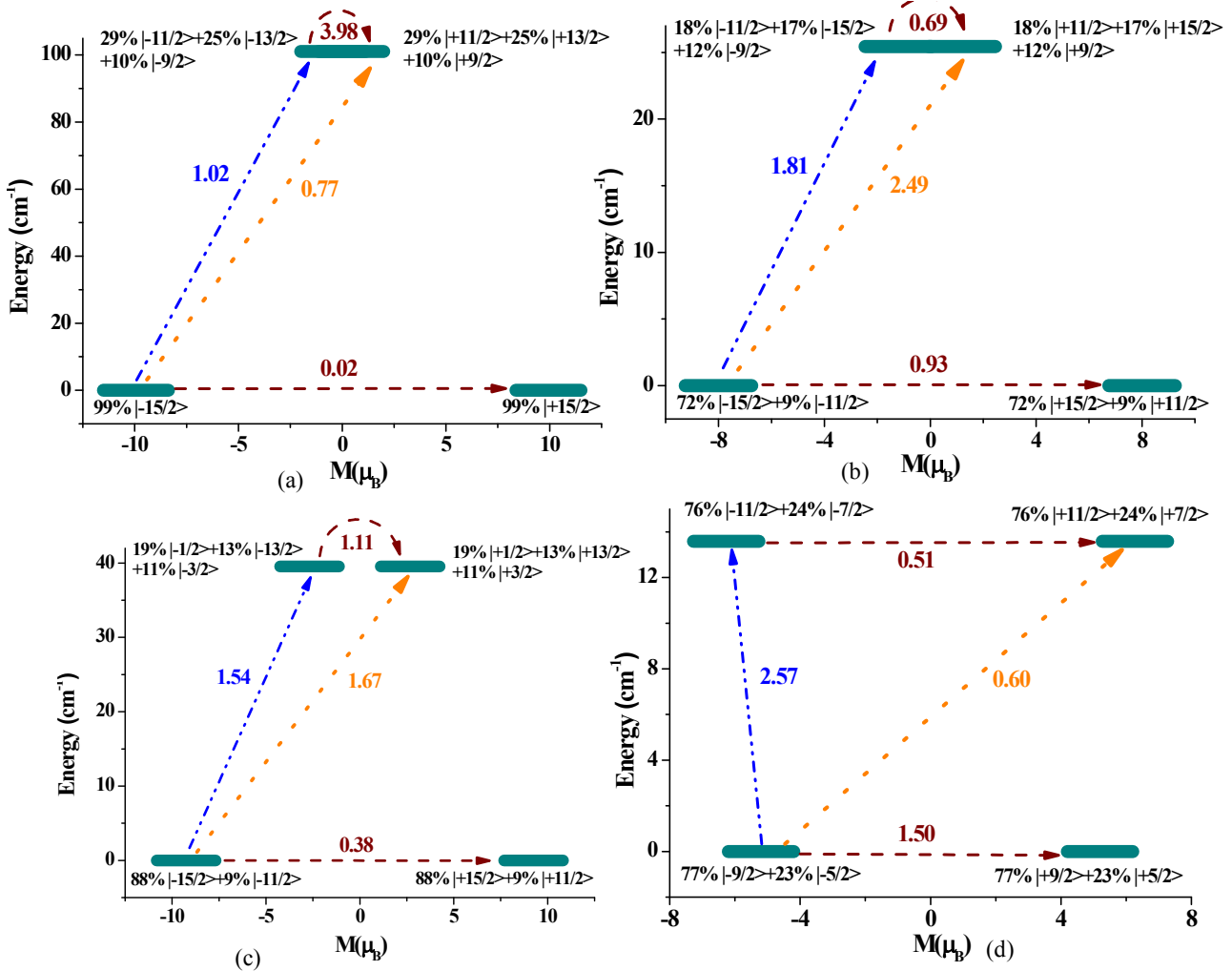


Figure S15. Ab initio computed Single-Ion based magnetization relaxation blockade for (a) Dy1 (b) Dy2a (c) Dy2b (d) Dy3 sites respectively in complex **2**.

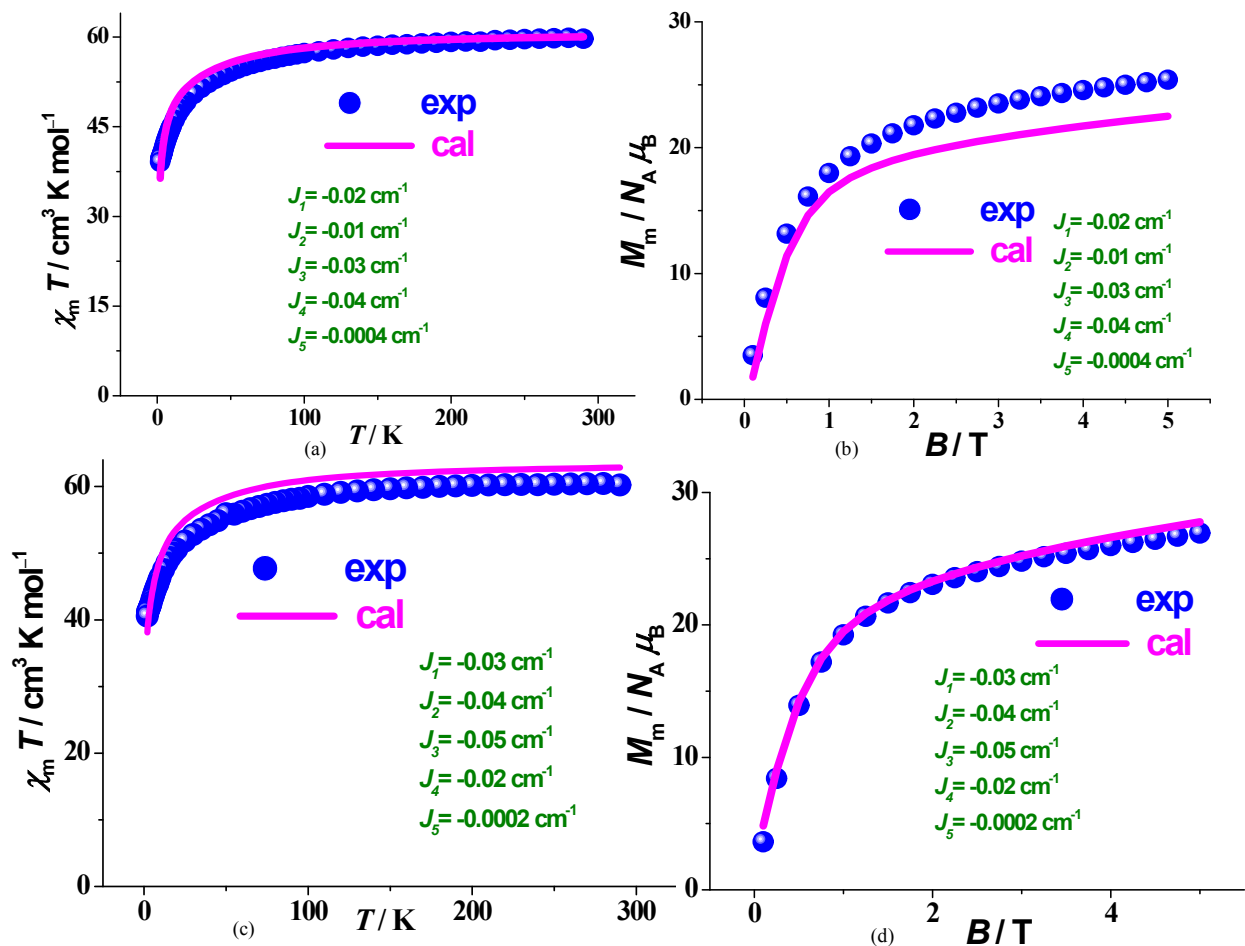
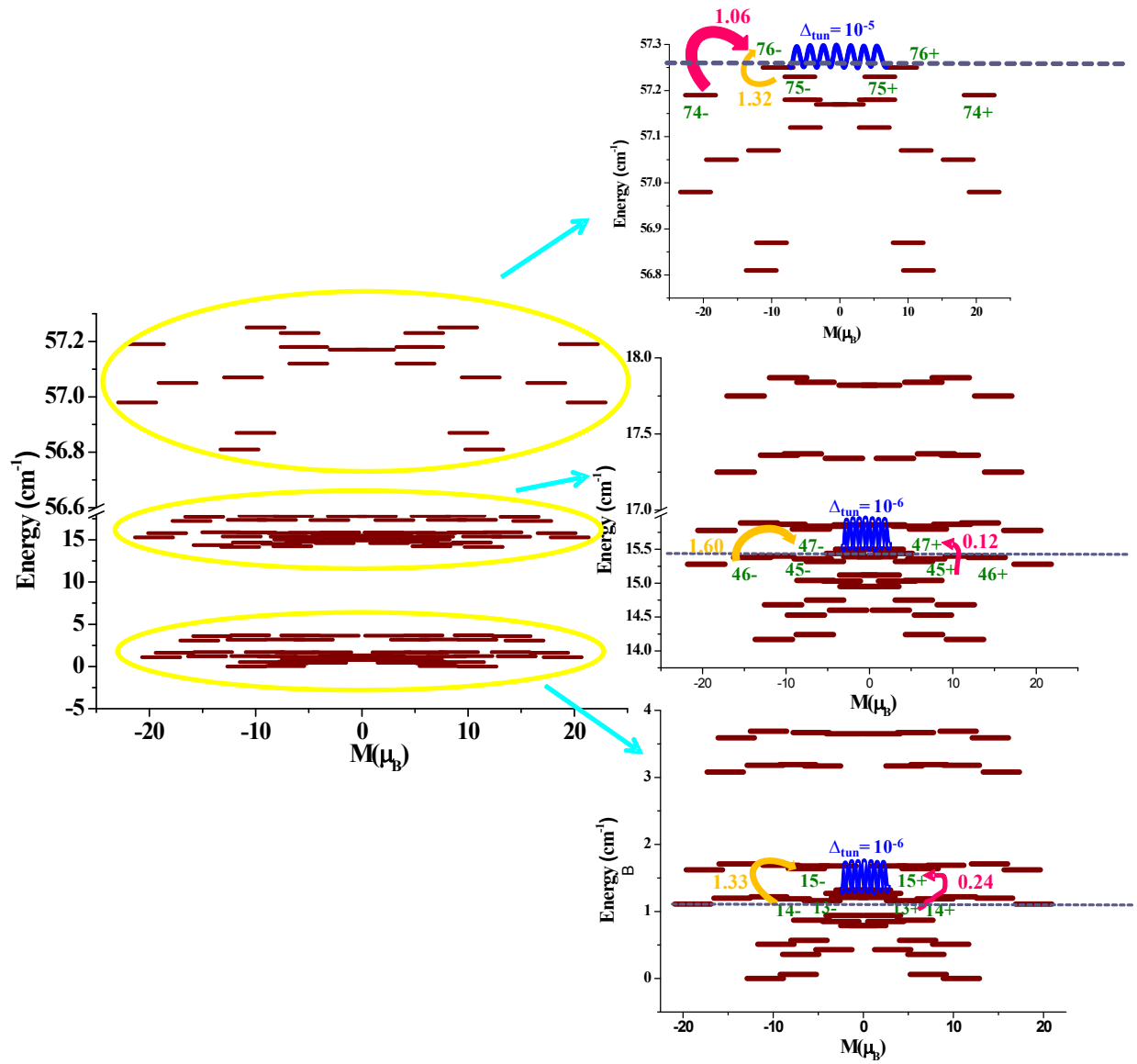
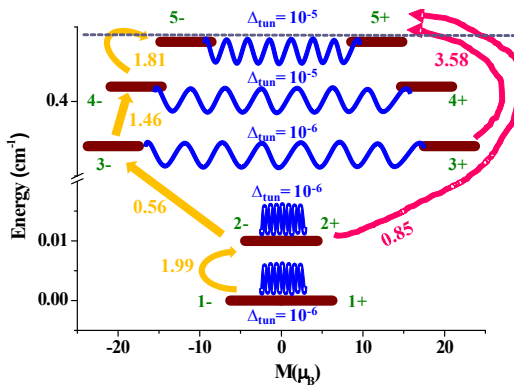


Figure S16. Temperature dependence $\chi_m T$ plot for complexes (a) **1**, (c) **2** and Field dependence molar magnetization plot for complexes (b) **1**, (d) **2**. Blue circle denote experimental data while solid lines correspond to *ab initio* simulations using five different exchange interactions and constant intermolecular interaction (zJ) of -0.0009 cm^{-1} .



(a)



(b)

Figure S17. Low lying exchange spectrum and position of the magnetization blockade barrier (grey dashed line) in complexes **1** (a) and **2** (b). The bold horizontal brown lines indicate exchange states which have been arranged in compliance with the value of its magnetic moment as sequentially represented by gradually increasing numbers (green texts). The blue curved arrows correspond to connecting same exchange doublets of reverse magnetization and imply direct QTM/TA-QTM contribution to the magnetic relaxation. The yellow straight/curved arrows infer to the spin-phonon transitions between an exchange doublet and its congener nearest-neighbour higher excited exchange doublets. Pink arrow reveals spin-phonon transition between lower exchange KDs to next-nearest neighbour exchange KDs. The numbers near each arrows represent corresponding transversal matrix elements for the transition magnetic moments of pertinent relaxation pathway.

Understanding relaxation mechanism in exchange-coupled system

In order to dissect the computed exchange coupled states, most probable relaxation pathways from maximum magnetized state of ground exchange doublet to the time reversed state with opposite magnetization (see Figure S17 and Tables S12 and S13)^{R7} need to be appraised. As discussed in single-ion discussion, relaxation pathway is essentially dictated by QTM and spin-phonon transition processes. QTM happens either via direct tunneling between two of reverse magnetization of a specific doublet or through indirect tunneling via excited states. In non-Kramers type of complex **1**, matrix element corresponding to direct QTM is zero ($\leq 10^{-8} \mu_B$) as per Griffith theorem. The direct QTM in **1** owes to intrinsic tunneling gap (Δ_{tun}) in absence of magnetic field. Hence, we will analyze tunnel gap between the exchange doublets as well as matrix elements pertinent to spin-phonon transitions to ascertain the magnetization blockade. We have forged the exchange spectrum (see Figure S17) where all the exchange states (brown horizontal lines) were arranged in conformation with pertinent maximum magnetic moments of

the exchange doublets. The numbers implying each arrow between any two energy states delineate root-mean-square value of matrix elements of magnetic moments (in μ_B).

Complex 1:

Small ground Δ_{tun} ($\sim 10^{-10} \text{ cm}^{-1} \ll \text{cut-off} = 10^{-5} \text{ cm}^{-1}$)^{R8} allows subsequent relaxation via excited states. $\Delta_{\text{tun}} = 10^{-6} \text{ cm}^{-1}$ between 13th, 14th and 15th exchange doublets (near cut-off) tends to channelize relaxation via these levels. Considerable transversal magnetic moment matrix elements corresponding to spin-phonon transition (yellow/pink arrows in Figure S17) between ± 14 and ± 15 states ($1.33/0.01 \mu_B$) as well as between ± 13 and ± 15 states ($0.24 \mu_B$; see Table S12 and Figure S17a) consolidates presumable relaxation via 15th exchange doublet outlining possible barrier as 1.22 cm^{-1} . Nevertheless, the tunneling contribution being smaller than the cut-off vouches for the presence of other relaxation mechanisms. Moving ahead above, replica of above mechanism is witnessed for 47th exchange doublet having $\Delta_{\text{tun}} = 10^{-6} \text{ cm}^{-1}$. Moving ahead above, replica of above mechanism is witnessed for 47th exchange doublet having $\Delta_{\text{tun}} = 10^{-6} \text{ cm}^{-1}$. Additionally, matrix elements for the spin-phonon transitions implicating ± 46 and ± 47 ($1.60 \mu_B$) as well as ± 45 and ± 47 ($0.12 \mu_B$) levels promote magnetization blockade at 47th state enumerating $U_{\text{cal}} = 15.38 \text{ cm}^{-1}$. Like earlier instance, smaller than cut-off value of tunneling gap unfolds more subsequent relaxations via higher levels. Tunnelling transition of 10^{-5} cm^{-1} at par with the cut-off value was detected between the ± 76 exchange doublet states (see Table S12). This value solely advocates for the blockage of magnetization at 76th exchange doublet with no further probability to move via higher levels. Eventual relaxation via 76th exchange doublet was further corroborated by matrix elements pertinent to spin-phonon transitions between ± 75 and ± 76 ($1.32 \mu_B$; yellow arrows)/ ± 74 and ± 76 ($1.06 \mu_B$; light pink arrows) (see Figure S17a) states. So, final possible U_{cal} can be enumerated to be 57.24 cm^{-1} (see Table S12 and Figure S17a).

Complex 2:

Considering overall non-Kramers nature of **2**, tunnel gap between exchange doublets is likely to be genesis of QTM contribution to magnetization relaxation while matrix elements corresponding to QTM process must be zero ($\sim 10^{-10} \mu_B$). Within ground state, $\Delta_{\text{tun}} = 10^{-6} \text{ cm}^{-1}$ provokes relaxation via higher energy state. Moving ahead, considerably large (close to cut-off) Δ_{tun} between ± 2 (blue arrows in Figure S17b) in conjunction with matrix elements corresponding to spin-phonon transitions ($1.99 \mu_B$) dictates small possible relaxation via this

state outlining $U_{\text{cal}} = 0.01 \text{ cm}^{-1}$ (see Figure S17b and Table S13). Subsequently, pronounced $\Delta_{\text{tun}} = 10^{-6} \text{ cm}^{-1}$ between ± 5 exchange states coupled with matrix elements belonging to spin-phonon transitions between $(\pm 4) - (\pm 5) / (\pm 3) - (\pm 5) / (\pm 2) - (\pm 5)$ as 1.81, 3.58 and $0.85 \mu_B$ articulate relaxation via fifth exchange doublet. This blocks magnetization at ± 5 state itself enumerating eventual $U_{\text{cal}} = 0.44 \text{ cm}^{-1}$ for **2** (see Figure S17b and Table S13). Small energy barrier of 0.01 cm^{-1} is extremely small to induce any SMM feature reproducing experimental trend of lack of SMM behavior in absence of magnetic field. Application of magnetic field to suppress tunnel splitting computationally leads to $U_{\text{cal}} = 0.44 \text{ cm}^{-1}$ which is also tiny to inflict SMM trait even in presence of magnetic field precluding SMM behavior solely in **2**.

Table S11. Parameters of the magnetic interaction in complexes **1–2**

Complex 1					
Type of magnetic interaction (in cm^{-1})	J_1	J_2	J_3	J_4	J_5
J_i^{dipolar}	-0.02	-0.04	+0.01	-0.04	-0.0002
J_i^{exch}	-0.02	-0.01	-0.03	-0.04	-0.0004
J_{tot}	-0.04	-0.05	-0.02	-0.08	-0.0006
zJ	-0.00009	-0.00009	-0.00009	-0.00009	-0.00009

Complex 2					
Type of magnetic interaction (in cm^{-1})	J_1	J_2	J_3	J_4	J_5
J_i^{dipolar}	-0.05	+0.00	-0.02	-0.04	+0.0001
J_i^{exch}	-0.03	-0.04	-0.05	-0.02	-0.0002
J_{tot}	-0.08	-0.04	-0.07	-0.06	-0.0001
zJ	-0.00009	-0.00009	-0.00009	-0.00009	-0.00009

Table S12. Energies (cm^{-1}), corresponding tunnel splitting (Δ_{tun}) g_z values of the low-lying exchange doublet states and corresponding magnetic moment matrix element values pertinent to various relaxation pathways in complex **1**

KD s	Energy(cm^{-1})	Main values of g tensor	$\Delta_{\text{tun}}(\text{cm}^{-1})$	Corresponding Matrix elements for	
				QTM	Spin-phonon transition

1	0.0000000 0.0000000	g_x	$\sim 10^{-8}$	10^{-10}	10^{-11}	
		g_y	$\sim 10^{-7}$			
		g_z	21.74			
2	0.0599762 0.0599762	g_x	$\sim 10^{-8}$	10^{-10}	10^{-11}	2.44, $\sim 10^{-7}$
		g_y	$\sim 10^{-7}$			
		g_z	21.04			
3	0.4260275 0.4260275	g_x	$\sim 10^{-8}$	10^{-10}	10^{-12}	0.09, $\sim 10^{-6}$
		g_y	$\sim 10^{-7}$			
		g_z	17.96			
4	0.5093965 0.5093965	g_x	$\sim 10^{-8}$	10^{-10}	10^{-11}	2.34, $\sim 10^{-7}$
		g_y	$\sim 10^{-8}$			
		g_z	27.63			
5	0.5745652 0.5745652	g_x	$\sim 10^{-7}$	10^{-10}	10^{-11}	$\sim 10^{-2}, \sim 10^{-6}$
		g_y	$\sim 10^{-7}$			
		g_z	19.96			
6	0.7860095 0.7860095	g_x	$\sim 10^{-7}$	10^{-9}	10^{-11}	2.36, $\sim 10^{-7}$
		g_y	$\sim 10^{-7}$			
		g_z	24.19			
7	0.8483647 0.8483647	g_x	$\sim 10^{-8}$	10^{-9}	10^{-11}	$10^{-5}, 10^{-1}$
		g_y	$\sim 10^{-8}$			
		g_z	27.36			
8	0.8707439 0.8707439	g_x	$\sim 10^{-8}$	10^{-9}	10^{-11}	$10^{-6}, \mathbf{1.95}$
		g_y	$\sim 10^{-7}$			
		g_z	42.06			
9	0.9414092 0.9414092	g_x	$\sim 10^{-8}$	10^{-9}	10^{-12}	$10^{-2}, 10^{-3}$
		g_y	$\sim 10^{-7}$			
		g_z	13.32			

10	1.1123513 1.1123514	g_x	$\sim 10^{-8}$	10^{-7}	10^{-12}	2.27 , $\sim 10^{-6}$
		g_y	$\sim 10^{-7}$			
		g_z	32.40			
11	1.1558539 1.1558546	g_x	$\sim 10^{-8}$	10^{-7}	10^{-12}	$10^{-5}, 10^{-2}$
		g_y	$\sim 10^{-7}$			
		g_z	42.29			
12	1.1907053 1.1907066	g_x	$\sim 10^{-7}$	10^{-6}	10^{-11}	0.30 , $\sim 10^{-3}$
		g_y	$\sim 10^{-7}$			
		g_z	22.98			
13	1.1989151 1.1989189	g_x	$\sim 10^{-8}$	10^{-6}	10^{-10}	0.03 , 0.07
		g_y	$\sim 10^{-7}$			
		g_z	24.68			
14	1.2084605 1.2084660	g_x	$\sim 10^{-8}$	10^{-6}	10^{-9}	2.15 , $\sim 10^{-2}$
		g_y	$\sim 10^{-8}$			
		g_z	51.89			
15	1.2211200 1.2211217	g_x	$\sim 10^{-8}$	10^{-6}	10^{-8}	1.33 , 0.01
		g_y	$\sim 10^{-8}$			
		g_z	29.22			
16	1.2706151 1.2706151	g_x	$\sim 10^{-8}$	10^{-8}	10^{-10}	0.03, 0.19
		g_y	$\sim 10^{-7}$			
		g_z	22.74			
17	1.3246365 1.3246365	g_x	$\sim 10^{-8}$	10^{-8}	10^{-12}	$10^{-2}, 10^{-4}$
		g_y	$\sim 10^{-8}$			
		g_z	25.56			
18	1.6195853 1.6195856	g_x	$\sim 10^{-8}$	10^{-7}	10^{-12}	$10^{-5}, \mathbf{2.01}$
		g_y	$\sim 10^{-8}$			
		g_z	39.93			

19	1.6401731 1.6401740	g_x	$\sim 10^{-8}$	10^{-7}	10^{-11}	$10^{-2}, 10^{-2}$
		g_y	$\sim 10^{-7}$			
		g_z	48.34			
20	1.6750504 1.6750511	g_x	$\sim 10^{-8}$	10^{-7}	10^{-10}	0.81, 10⁻²
		g_y	$\sim 10^{-9}$			
		g_z	24.01			
21	1.6848638 1.6848663	g_x	$\sim 10^{-8}$	10^{-6}	10^{-11}	0.02, 0.07
		g_y	$\sim 10^{-8}$			
		g_z	23.56			
22	1.6971062 1.6971094	g_x	$\sim 10^{-8}$	10^{-6}	10^{-9}	0.07, 0.02
		g_y	$\sim 10^{-8}$			
		g_z	25.43			
23	1.7135053 1.7135062	g_x	$\sim 10^{-10}$	10^{-6}	10^{-10}	0.04, 0.20
		g_y	$\sim 10^{-8}$			
		g_z	18.95			
24	3.0834618 3.0834618	g_x	$\sim 10^{-7}$	10^{-9}	10^{-10}	0.46, 0.03
		g_y	$\sim 10^{-6}$			
		g_z	56.17			
25	3.0834618 3.0834618	g_x	$\sim 10^{-8}$	10^{-9}	10^{-13}	$10^{-4}, 10^{-4}$
		g_y	$\sim 10^{-8}$			
		g_z	54.12			
26	3.1714040 3.1714041	g_x	$\sim 10^{-7}$	10^{-7}	10^{-11}	$10^{-4}, \mathbf{0.74}$
		g_y	$\sim 10^{-7}$			
		g_z	33.14			
27	3.1777182 3.1777183	g_x	$\sim 10^{-7}$	10^{-7}	10^{-11}	$10^{-4}, \mathbf{3.28}$
		g_y	$\sim 10^{-7}$			
		g_z	60.65			

28	3.1916860 3.1916860	g_x	$\sim 10^{-7}$	10^{-9}	10^{-11}	$10^{-3}, \mathbf{0.74}$
		g_y	$\sim 10^{-6}$			
		g_z	18.02			
29	3.5903243 3.5903243	g_x	$\sim 10^{-7}$	10^{-9}	10^{-12}	$10^{-6}, 0.04$
		g_y	$\sim 10^{-6}$			
		g_z	54.56			
30	3.6544441 3.6544442	g_x	$\sim 10^{-7}$	10^{-7}	10^{-11}	$10^{-3}, \mathbf{0.33}$
		g_y	$\sim 10^{-7}$			
		g_z	29.74			
31	3.6691835 3.6691836	g_x	$\sim 10^{-7}$	10^{-7}	10^{-12}	$10^{-4}, \mathbf{2.46}$
		g_y	$\sim 10^{-6}$			
		g_z	20.89			
32	3.6922640 3.6922641	g_x	$\sim 10^{-7}$	10^{-7}	10^{-12}	$10^{-3}, \mathbf{0.23}$
		g_y	$\sim 10^{-7}$			
		g_z	67.00			
33	14.1667991 14.1667991	g_x	$\sim 10^{-7}$	10^{-10}	10^{-13}	$10^{-6}, 10^{-6}$
		g_y	$\sim 10^{-6}$			
		g_z	22.94			
34	14.2364387 14.2364387	g_x	$\sim 10^{-7}$	10^{-10}	10^{-13}	$10^{-7}, \mathbf{2.55}$
		g_y	$\sim 10^{-6}$			
		g_z	20.33			
35	14.5290310 14.5290310	g_x	$\sim 10^{-7}$	10^{-10}	10^{-12}	$10^{-6}, 0.08$
		g_y	$\sim 10^{-7}$			
		g_z	19.02			
36	14.6023765 14.6023765	g_x	$\sim 10^{-6}$	10^{-10}	10^{-12}	$10^{-7}, \mathbf{2.35}$
		g_y	$\sim 10^{-6}$			
		g_z	27.26			

37	14.6764517 14.6764517	g_x	$\sim 10^{-8}$	10^{-10}	10^{-12}	$10^{-5}, 10^{-2}$
		g_y	$\sim 10^{-8}$			
		g_z	21.32			
38	14.7507867 14.7507867	g_x	$\sim 10^{-8}$	10^{-10}	10^{-12}	$10^{-7}, \mathbf{2.41}$
		g_y	$\sim 10^{-7}$			
		g_z	23.41			
39	14.9502686 14.9502686	g_x	$\sim 10^{-8}$	10^{-9}	10^{-11}	$10^{-5}, 0.07$
		g_y	$\sim 10^{-8}$			
		g_z	26.98			
40	15.0271233 15.0271233	g_x	$\sim 10^{-8}$	10^{-9}	10^{-11}	$10^{-6}, \mathbf{1.82}$
		g_y	$\sim 10^{-7}$			
		g_z	42.47			
41	15.0381338 15.0381338	g_x	$\sim 10^{-8}$	10^{-9}	10^{-12}	$10^{-2}, 10^{-3}$
		g_y	$\sim 10^{-7}$			
		g_z	19.59			
42	15.1172769 15.1172769	g_x	$\sim 10^{-8}$	10^{-10}	10^{-12}	$10^{-6}, \mathbf{2.20}$
		g_y	$\sim 10^{-7}$			
		g_z	31.88			
43	15.2753127 15.2753128	g_x	$\sim 10^{-8}$	10^{-7}	10^{-12}	$10^{-5}, 10^{-2}$
		g_y	$\sim 10^{-8}$			
		g_z	50.06			
44	15.3198181 15.3198186	g_x	$\sim 10^{-8}$	10^{-7}	10^{-11}	$10^{-3}, \mathbf{0.29}$
		g_y	$\sim 10^{-8}$			
		g_z	22.81			
45	15.3594032 15.3594039	g_x	$\sim 10^{-8}$	10^{-7}	10^{-11}	$0.06, 10^{-2}$
		g_y	$\sim 10^{-7}$			
		g_z	21.97			

46	15.3792013 15.3792055	g_x	$\sim 10^{-8}$	10^{-6}	10^{-9}	0.87, 10⁻²
		g_y	$\sim 10^{-7}$			
		g_z	52.57			
47	15.3875093 15.3875174	g_x	$\sim 10^{-8}$	10^{-6}	10^{-8}	1.60, 0.02
		g_y	$\sim 10^{-7}$			
		g_z	29.66			
48	15.3955395 15.3955431	g_x	$\sim 10^{-8}$	10^{-6}	10^{-10}	0.30, 0.07
		g_y	$\sim 10^{-7}$			
		g_z	24.46			
49	15.4351554 15.4351555	g_x	$\sim 10^{-8}$	10^{-8}	10^{-13}	$10^{-3}, 10^{-2}$
		g_y	$\sim 10^{-8}$			
		g_z	25.23			
50	15.5030691 15.5030691	g_x	$\sim 10^{-8}$	10^{-9}	10^{-12}	$10^{-5}, \mathbf{1.87}$
		g_y	$\sim 10^{-8}$			
		g_z	38.34			
51	15.7829291 15.7829295	g_x	$\sim 10^{-8}$	10^{-7}	10^{-11}	$10^{-2}, 10^{-2}$
		g_y	$\sim 10^{-7}$			
		g_z	49.36			
52	15.8045383 15.8045391	g_x	$\sim 10^{-8}$	10^{-7}	10^{-11}	$0.77, 10^{-2}$
		g_y	$\sim 10^{-8}$			
		g_z	23.95			
53	15.8438218 15.8438224	g_x	$\sim 10^{-8}$	10^{-7}	10^{-11}	$0.06, 10^{-2}$
		g_y	$\sim 10^{-7}$			
		g_z	22.31			
54	15.8634453 15.8634486	g_x	$\sim 10^{-8}$	10^{-6}	10^{-9}	$0.04, 0.05$
		g_y	$\sim 10^{-8}$			
		g_z	25.89			

55	15.8712079 15.8712119	g_x	$\sim 10^{-8}$	10^{-6}	10^{-10}	0.02, 0.31
		g_y	$\sim 10^{-8}$			
		g_z	20.66			
56	15.8937010 15.8937017	g_x	$\sim 10^{-10}$	10^{-7}	10^{-10}	0.35, 0.03
		g_y	$\sim 10^{-10}$			
		g_z	55.55			
57	17.2464585 17.2464585	g_x	$\sim 10^{-7}$	10^{-9}	10^{-12}	$10^{-4}, 10^{-4}$
		g_y	$\sim 10^{-7}$			
		g_z	54.94			
58	17.3401467 17.3401467	g_x	$\sim 10^{-8}$	10^{-8}	10^{-11}	$10^{-4}, 0.24$
		g_y	$\sim 10^{-10}$			
		g_z	30.12			
59	17.3578217 17.3578217	g_x	$\sim 10^{-8}$	10^{-8}	10^{-11}	$10^{-4}, 1.13$
		g_y	$\sim 10^{-7}$			
		g_z	63.50			
60	17.3662231 17.3662232	g_x	$\sim 10^{-8}$	10^{-8}	10^{-12}	$10^{-3}, 0.25$
		g_y	$\sim 10^{-8}$			
		g_z	19.16			
61	17.7538582 17.7538582	g_x	$\sim 10^{-8}$	10^{-9}	10^{-11}	$10^{-5}, 0.04$
		g_y	$\sim 10^{-6}$			
		g_z	55.47			
62	17.8236145 17.8236146	g_x	$\sim 10^{-8}$	10^{-8}	10^{-11}	$10^{-3}, 0.23$
		g_y	$\sim 10^{-7}$			
		g_z	31.18			
63	17.8428854 17.8428855	g_x	$\sim 10^{-8}$	10^{-8}	10^{-12}	$10^{-4}, \mathbf{2.32}$
		g_y	$\sim 10^{-7}$			
		g_z	20.03			

64	17.8722732 17.8722732	g_x	$\sim 10^{-8}$	10^{-8}	10^{-11}	$10^{-3}, 0.13$
		g_y	$\sim 10^{-7}$			
		g_z	66.48			
65	56.8058279 56.8058279	g_x	$\sim 10^{-8}$	10^{-8}	10^{-12}	$10^{-6}, 10^{-6}$
		g_y	$\sim 10^{-7}$			
		g_z	24.73			
66	56.8654395 56.8654396	g_x	$\sim 10^{-7}$	10^{-8}	10^{-12}	$10^{-5}, \mathbf{2.51}$
		g_y	$\sim 10^{-6}$			
		g_z	31.83			
67	56.9751658 56.9751659	g_x	$\sim 10^{-8}$	10^{-7}	10^{-12}	$10^{-4}, 0.63$
		g_y	$\sim 10^{-7}$			
		g_z	44.87			
68	57.0475027 57.0475032	g_x	$\sim 10^{-7}$	10^{-6}	10^{-12}	$10^{-4}, \mathbf{2.41}$
		g_y	$\sim 10^{-6}$			
		g_z	42.10			
69	57.0693787 57.0693793	g_x	$\sim 10^{-7}$	10^{-6}	10^{-12}	$0.83, 10^{-2}$
		g_y	$\sim 10^{-6}$			
		g_z	23.47			
70	57.1153175 57.1153177	g_x	$\sim 10^{-7}$	10^{-7}	10^{-12}	$10^{-4}, \mathbf{2.31}$
		g_y	$\sim 10^{-6}$			
		g_z	24.90			
71	57.1712531 57.1712550	g_x	$\sim 10^{-8}$	10^{-6}	10^{-12}	$\mathbf{2.29}, 10^{-3}$
		g_y	$\sim 10^{-8}$			
		g_z	15.14			
72	57.1751135 57.1751142	g_x	$\sim 10^{-7}$	10^{-6}	10^{-9}	$\mathbf{2.36}, 10^{-2}$
		g_y	$\sim 10^{-5}$			
		g_z	15.25			

73	57.1764744 57.1764753	g_x	$\sim 10^{-8}$	10^{-7}	10^{-9}	$10^{-2}, \mathbf{3.19}$
		g_y	$\sim 10^{-6}$			
		g_z	14.23			
74	57.1934793 57.1934816	g_x	$\sim 10^{-8}$	10^{-6}	10^{-11}	$10^{-2}, 0.28$
		g_y	$\sim 10^{-8}$			
		g_z	47.57			
75	57.2264062 57.2264117	g_x	$\sim 10^{-8}$	10^{-6}	10^{-11}	0.22, 0.02
		g_y	$\sim 10^{-7}$			
		g_z	19.31			
76	57.2489318 57.2489442	g_x	$\sim 10^{-8}$	10^{-5}	10^{-10}	$1.32, 10^{-2}$
		g_y	$\sim 10^{-7}$			
		g_z	23.13			

Table S13. Energies (cm^{-1}), corresponding tunnel splitting (Δ_{tun}) g_z values of the low-lying exchange doublet states and corresponding magnetic moment matrix element values pertinent to various relaxation pathways in complex **2**

KDs	Energy(cm^{-1})	Main values of g tensor		$\Delta_{\text{tun}} (\text{cm}^{-1})$	Corresponding Matrix elements for	
					QTM	Spin-phonon transition
1	0.0000000 0.0000023	g_x	$\sim 10^{-8}$	10^{-6}	$\sim 10^{-10}$	-
		g_y	$\sim 10^{-8}$			
		g_z	6.25			
2	0.0102820 0.0102831	g_x	$\sim 10^{-8}$	10^{-6}	$\sim 10^{-9}$	$1.99, \sim 10^{-3}$
		g_y	$\sim 10^{-8}$			
		g_z	17.92			
3	0.3711558 0.3711652	g_x	$\sim 10^{-8}$	10^{-6}	$\sim 10^{-10}$	$0.56, \sim 10^{-2}$
		g_y	$\sim 10^{-8}$			
		g_z	49.29			
4	0.4096685 0.4096916	g_x	$\sim 10^{-8}$	10^{-5}	$\sim 10^{-10}$	$1.46, \sim 10^{-2}$
		g_y	$\sim 10^{-7}$			
		g_z	44.11			
5	0.4409771	g_x	$\sim 10^{-8}$	10^{-5}	$\sim 10^{-9}$	$1.81, 0.02$

	0.4410115	g_y	$\sim 10^{-8}$			
		g_z	29.63			

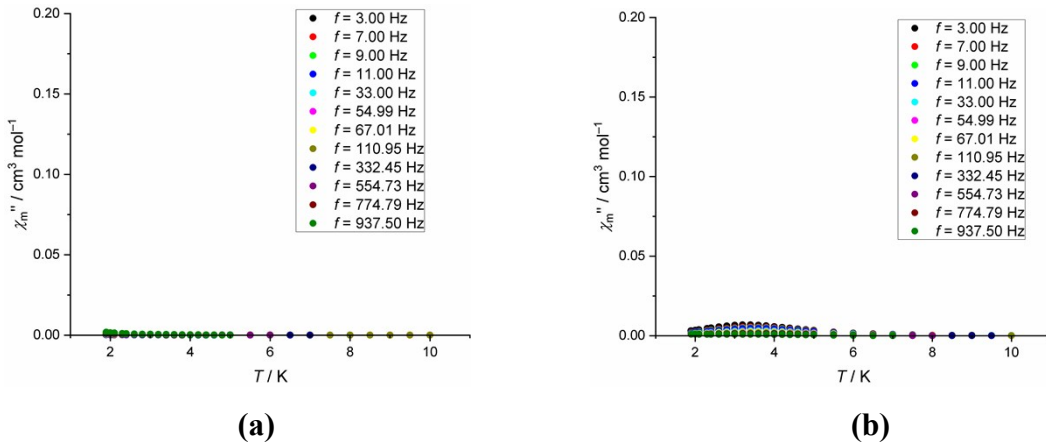


Figure S18. Plot of χ_m'' versus T at the frequencies indicated for **2** under (a) zero static bias field and (b) 0.2 Tesla bias field.

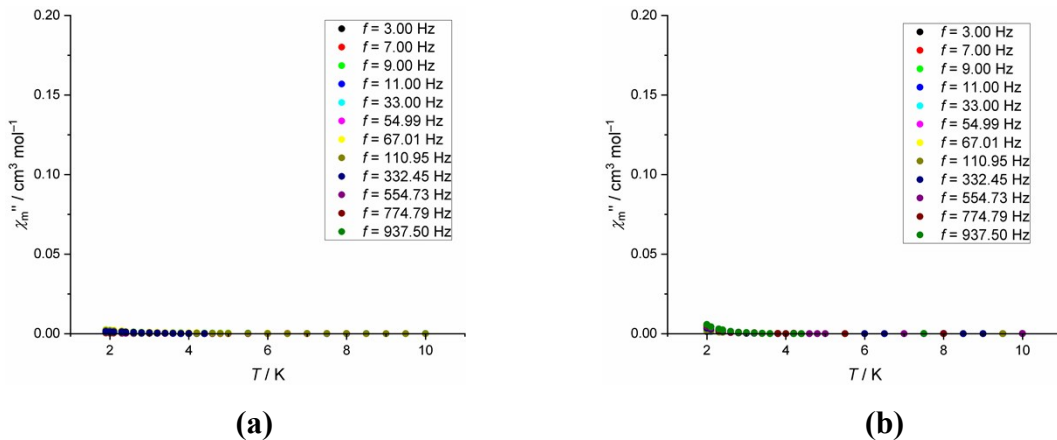


Figure S19. Plot of χ_m'' versus T at the frequencies indicated for **3** under (a) zero static bias field and (b) 0.2 Tesla bias field.

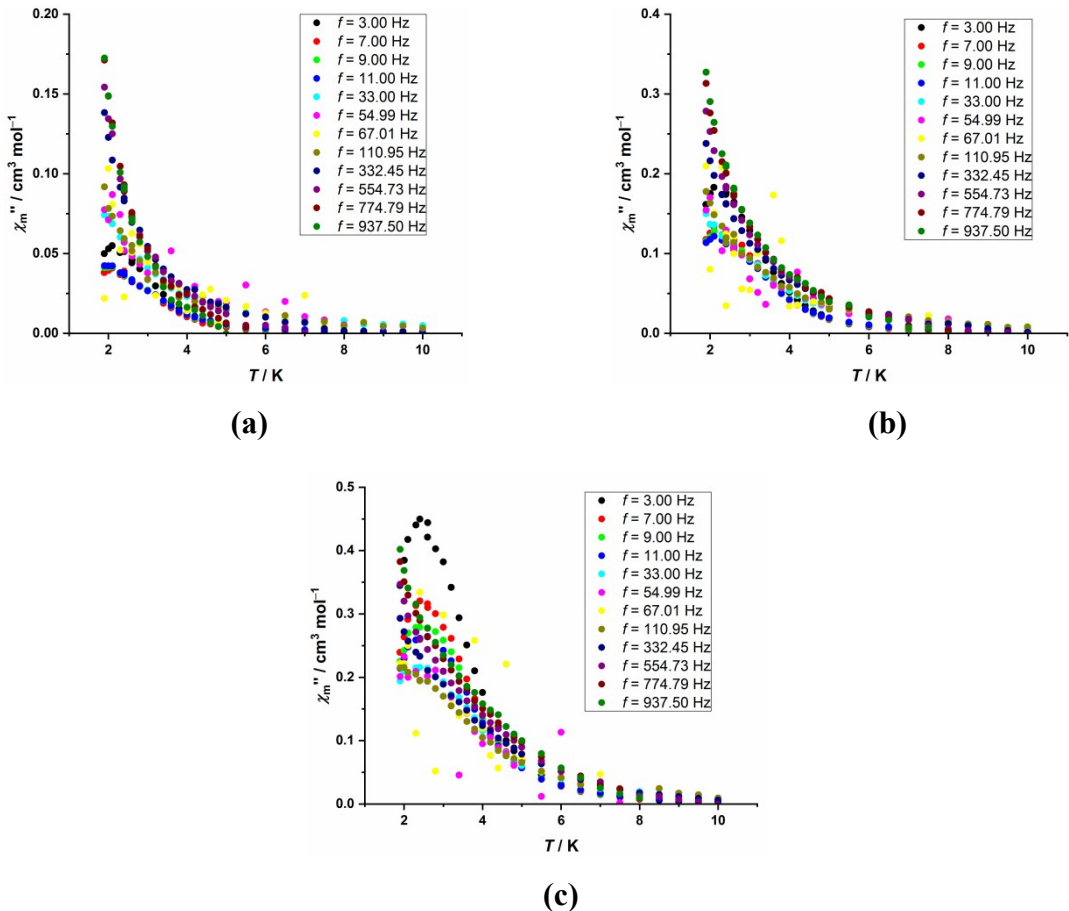


Figure S20. Plot of χ_m'' versus T at the frequencies indicated for **1** under (a) 0.05 Tesla, (b) 0.1 Tesla and (c) 0.2 Tesla static bias fields. From 0.2 Tesla onwards the Zeeman effect becomes prominent affecting the nature of the curves.

References

- R1. B. O. Roos and P.-Å. Malmqvist, *Phys. Chem. Chem. Phys.*, 2004, **6**, 2919–2927.
- R2. P.-Å. Malmqvist, B. O. Roos and B. Schimmelpfennig, *Chem. Phys. Lett.*, 2002, **357**, 230–240.
- R3. (a) F. Aquilante, J. Autschbach, R. K. Carlson, L. F. Chibotaru, M. G. Delcey, L. D. Vico, I. F. Galván, N. Ferré, L. M. Frutos, L. Gagliardi, M. Garavelli, A. Giussani, C. E. Hoyer, G. L. Manni, H. Lischka, D. Ma, P. Å. Malmqvist, T. Müller, A. Nenov, M. Olivucci, T. B. Pedersen, D. Peng, F. Plasser, B. Pritchard, M. Reiher, I. Rivalta, I. Schapiro, J. S.- Martí, M. Stenrup, D. G. Truhlar, L. Ungur, A. Valentini, S. Vancoillie, V. Veryazov, V. P. Vysotskiy, O. Weingart, F. Zapata and R. Lindh, *J. Compt. Chem.*, 2016, **37**, 506–541. (b) F. Aquilante, L. D. Vico, N. Ferre, G. Ghigo, P. A. Malmqvist, P. Neogrady, T. B. Pedersen, M. Pitonak, M. Reiher, B. O.

Roos, L. S.- Andres, M. Urban, V. Veryazov and R. Lindh, *J. Comput. Chem.*, 2010, **31**, 224–247. (c) J. A. Duncan, *J. Am. Chem. Soc.*, 2009, **131**, 2416–2416. (d) V. Veryazov, P. O. Widmark, L. S.- Andres, R. Lindh and B. O. Roos, *Int. J. Quantum Chem.*, 2004, **100**, 626–635. (e) G. Karlstrom, R. Lindh, P. A. Malmqvist, B. O. Roos, U. Ryde, V. Veryazov, P. O. Widmark, M. Cossi, B. Schimmelpfennig, P. Neogrady and L. Seijo, *Comput. Mater. Sci.*, 2003, **28**, 222–239.

R4. L. F. Chibotaru and L. Ungur, *J. Chem. Phys.*, 2012, **137**, 064112–064112.

R5. S. K. Langley, L. Ungur, N. F. Chilton, B. Moubaraki, L. F. Chibotaru, K. S. Murray, *Inorg. Chem.*, 2014, **53**, 4303–4315.

R6. (a) L. Ungur, W. V. d. Heuvel and L. F. Chibotaru, *New J. Chem.*, 2009, **33**, 1224–1230. (b) L. F. Chibotaru, L. Ungur and A. Soncini, *Angew. Chem., Int. Ed.*, 2008, **47**, 4126–4129.

R7. L. Ungur, M. Thewissen, J.-P. Costes, W. Wernsdorfer and L. F. Chibotaru, *Inorg. Chem.*, 2013, **52**, 6328–6337.

R8. L. F. Chibotaru, L. Ungur, C. Aronica, H. Elmoll, G. Pilet and D. Luneau, *J. Am. Chem. Soc.*, 2008, **130**, 12445–12455.